Probabilistic Analysis of Near-field Blast Loads Considering Fireball

Surface Instabilities and Stochastic Detonator Location

3 Ye Hu^a, Yanchao Shi^{a,*}, S.E. Rigby^b, Li Chen^c

4 a Key Laboratory of Coast Civil Structural Safety of the Ministry of Education, Tianjin University, Tianjin 300350,

5 China

b Department of Civil & Structural Engineering, University of Sheffield, Mappin Street, Sheffield, S1 3JD, UK

7 c Engineering Research Center of Safety and Protection of Explosion & Impact of Ministry of Education,

8 Southeast University, Nanjing 211189, China

9 10

1

2

* The corresponding author: Yanchao Shi; Email address: yanchaoshi@tju.edu.cn.

11

12

13

14

15

16

17

18

19

20

21

22

23

24

25

26

27

28

29

30

31

Abstract: High speed video analysis of near-field explosive detonations displays distinct stages of emergent hydrodynamic instabilities in the fireball/shock-air interface. Typically, beyond 10 charge radii, the instabilities experienced large growths giving rise to more chaotic behaviour of the interface and thus an increasing uncertainty in surface velocity. These surface instabilities are suggested as the primary cause of blast parameter variability in the near-field. However, as a deterministic tool, numerical simulation of the detonation process and subsequent blast wave propagation is not able to replicate the stochastic nature of fireball surface instabilities and hence near-field blast parameter variability. Therefore, it is necessary to develop new methods to simulate and characterise the stochastic features of the fireball/shock-air interface. This paper proposes an algorithm to generate an explosive charge element with random shape in finite element model in order to simulate irregularities in the fireball/shock-air interface, and therefore produce variabilities comparable to those from direct observation. The effect of chaotic fireball/shock-air interface on near-field loading is explored through a large number of numerical simulations in order to investigate the statistical distribution of parameters including peak overpressure and impulse. Subsequently, the effect of stochastic detonator location is explored in a similar manner. A computational procedure based on the Monte Carlo Method is proposed to establish a probabilistic model of near-field blast loads, termed PSL-Blast. The reliability of design blast loads calculated using the

33	reliability decreases with decreasing scaled distance. Finally, reliability-based safety
34	factors of blast loads are calculated based on different blast settings.
35	
36	Keyword: Near-field Blast loads; Probabilistic model; Fireball Surface Instability;
37	Safety factor.
38	
39	
40	
41	
42	
43	
44	
45	
46	
47	
48	
49	
50	
51	
52	
53	
54	
55	
56	
57	
58	
59	
60	

UFC 3-340-02 design manual is then estimated using PSL-Blast, which suggests that

1 Introduction

61

62

63

64

65

66

67

68

69

70

71

72

73

74

75

76

77

78

79

80

81

82

83

84

85

86

87

88

89

90

As a critical design step, the determination of blast loads is of paramount importance for the design of building structures for resilience and robustness. Prediction of blast loading is typically evaluated using the empirical formulas proposed by Kingery and Bulmash [1], hereafter shortened to KB, themselves derived from a large database of existing experimental trials. The KB method assumes the condition of either spherical centrally-initiated charges for free air bursts or hemispherical centrally-initiated charges for surface bursts. As a result, the KB method is widely recognised as an effective fast-running predictive tool for positive phase blast load parameters, and has been implemented into the UFC 3-340-02 design manual [2], the predictive computer code ConWep [3], and commercial finite element code LS-DYNA [4], among others. Meanwhile, considerable research effort [5-8] has been dedicated to the comparison of experimental results to KB predictions. Such previous studies have demonstrated varying levels of agreement with KB predictions, which is mainly attributed to large test-to-test variations in experimental measurements of blast load parameters and difficulties in establishing a reliable experimental benchmark. It is also observed that blast load variability reduces in well-controlled experimental trials but is not eliminated [9], emphasizing the requirement of variability quantification and its inclusion into predictive methods for more accurate prescribed loading conditions.

Research [10-14] into blast parameter variability, particularly with respect to scaled distance (given as the distance from the explosive divided by the cube-root of charge mass), has become an increasingly active area of research. Three distinct ranges of scaled distances are defined by Tyas [15] to estimate the variability degree of blast parameter, which concludes that the recorded blast parameter is highly repeatable and consistent at the extreme near-field (≤0.5 m/kg¹/³) and far-field scaled distances (≥2 m/kg¹/³), but higher variability of blast parameter is observed in the intermediate distances (0.5-2 m/kg¹/³). Meanwhile, Rae et al. [16] experimentally tested ground-detonated large hemispheres of C-4 to measure blast load parameters at scaled distances between 0.5 and 1.8 m/kg¹/³ and noted the presence of three similar regions. Results from the statistical analysis of 325 Mark-83 general purpose

conventional bombs conducted by Twisdale et al. [17] shows that the coefficient of variation (COV) of peak overpressure and impulse is 0.30 and 0.25, respectively. Low et al. [18] found a COV of 0.32 for peak reflected overpressure under various scaled distances based on the existing available data. The statistic result from 190 blast tests involving TNT, C-4 and ANFO explosives [19] shows a COV of 0.23 for peak reflected pressure within the scaled distances of 1.2 to 15.9 m/kg^{1/3}. Netherton et al. [20] developed a probabilistic model of blast parameter variability considering the combination of uncertain factors and the calculation result of exceeding probability for the design values of blast load generally reveals an over-estimation in the prediction of actual blast loads on a structure. Rigby et al. [21] compared the results from explosive trials with numerical analyses and concluded that PE4 has a consistent TNT equivalence value of 1.20 in the range of scaled distance 6.0-14.9 m/kg^{1/3}, and that blast parameter variability decreased as the situation approached the far-field. Meanwhile, Rigby et al. [22] quantified the variability associated with each blast parameter from highly controlled experimental recordings when compared to KB predictions, and grouped results from nominally identical tests. The presented results and the KB predictions held high levels of agreement, exhibiting variability of between $\pm 6-8\%$ for pressure and specific impulse parameters, $\pm 2.5\%$ for shock front arrival time and around $\pm 9\%$ for positive phase duration.

91

92

93

94

95

96

97

98

99

100

101

102

103

104

105

106

107

108

109

110

111

112

113

114

115

116

117

118

119

120

Furthermore, as observed in the detonation product cloud from the 1985 Minor Scale detonation [23], a stochastic distribution of detonation products results in, or at least amplifies, emergent instabilities in the fireball/shock-air interface. This performance is widely accepted to be the main reason for the blast parameter variability. Bogosian et al. [24] carried out blast tests of 11 cylindrical charges, and pressure-time histories were recorded and compared with that reported by Ohrt et al. [25] in the range of scaled distance 0.6 and 3.4 m/kg^{1/3}. The propensity for an expanding fireball to form instabilities was studied in the experimental work of Rigby et al. [26] using high speed video. The measured velocity behaviour showed two distinct stages of emergent instabilities in the fireball/shock-air interface. In the early stage after detonation, prior to or shortly after the emergence of small

turbulence-based instabilities, the fireball/air interface was observed to expand with effectively deterministic velocity. Beyond 10 charge radii, the instabilities experienced large growths giving rise to more chaotic behaviour of the interface and thus an increasing uncertainty in surface velocity. Tyas et al. [23] and Schoutens [27] both observed significant localised changes in blast parameter quantification on reflected surfaces as a direct result of instability formation.

Previous work has suggested that blast parameter variability is associated with Rayleigh-Taylor (RT) [28, 29] and Richtmyer-Meshkov (RM) [30, 31] instabilities. RT instabilities occur when pressure and density gradients are in opposite directions, and RM instabilities occur when a shock wave propagates through inhomogeneous media. In general, numerical simulation of blast shock wave is not able to reflect the surface instability performance of fireball/shock front and the induced blast parameter variability as a deterministic research method. The question of how to characterise the instability features of fireball/shock-air interface in a numerical model is challenging and is likely to be a highly meaningful contribution to stochastic studies of near-field blast loads.

This paper is organised in the following manner. First, an algorithm is developed in order to generate charge elements with random shape in a finite element. Subsequently, the effect of a statistically-varying fireball/shock-air interface on near-field explosion is investigated through a large number of numerical simulations. Additionally, the effect of random detonator location on the near-field explosion is also investigated. A computational procedure based on the Monte Carlo Method is proposed to establish a probabilistic model of near-field blast loads, termed *PSL-Blast*. This is then used to assess the reliability of design blast loads determined by UFC 3-340-02. Finally, a number of reliability-based safety factors of blast loads are for different blast settings.

2 Numerical simulation of near-field explosion

2.1 Model development

There are numerous techniques for modelling blast response of structures currently available in FE software. In particular, LS-DYNA includes four main methods:

ConWep LBE (*LOAD_BLAST_ENHANCED) [32]; MM-ALE (Multi Material Arbitrary Lagrange Euler) [33]; SPH (Smooth Particle Hydrodynamics) [34] and; CPM (Corpuscular Particle Method) [35]. The MM-ALE method draws on the respective advantages of Lagrangian and Eulerian methods. Namely, the ALE method first solves the problem in a pure Lagrangian framework by the processing of structural boundary motion, so it can effectively track movement of a material structural boundary. Following this, the mesh is transported back to its pre-deformed position in an Eulerian framework, such that large mesh deformations are avoided. This method is very advantageous in the analysis of large deformation problems, and an ALE mesh can define air and explosives with arbitrary charge shapes. Therefore, the MM-ALE method has clear advantages in the computation of numerical simulation of blast loads [36], particularly when considering surface imperfections and detonator location.

In this study, the MM-ALE method [33] was employed to model the blast wave formation and its interaction with a reflected surface. Furthermore, in order to decrease the required computation time, LS-DYNA's mapping capability is utilised [37-39], with an example shown in Fig. 1.

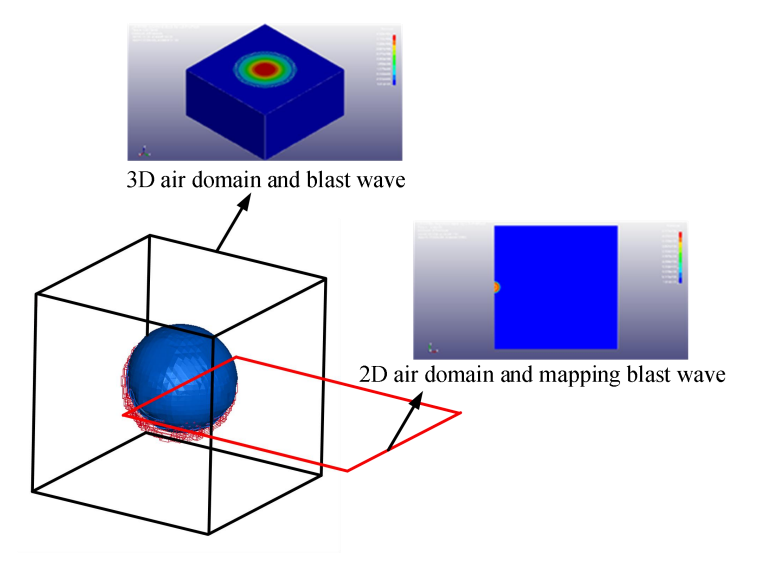
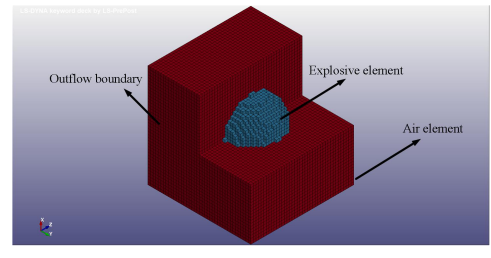


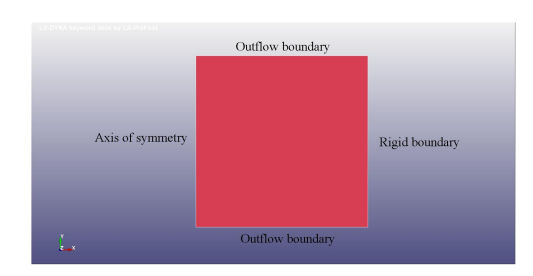
Fig. 1 3dto2d mapping program

The established FE model consists of two parts, including 3D FE model and

mapping 2D FE model. The existing study [37] shows the mesh variation ratio (mesh variation ratio = mesh length before mapping model under mesh length after mapping model) has an influence on the blast wave. It is known that for an acceptable peak overpressure during mapping to be obtained, the mesh variation ratio should be kept smaller than 10 [37]. Meanwhile, previous studies [39] showed that a numerical simulation with mesh size of 5 mm in the 2D FE model achieves sufficient accuracy and efficiency. Based on the reason above, a mesh size of 5 mm is chosen as mesh size in both the 3D FE model and 2D FE model. As shown in Fig. 2 (a), air and TNT explosive are directly modelled by solid elements for 3D analyses. The keyword *INITIAL_DETONATION defines the exact location of the explosive detonation. The boundary condition of the Eulerian mesh is set as an outflow boundary. Furthermore, 2D square shell elements (4-noded fully integrated quadrilateral shell elements) at the mapping step is shown in Fig. 2 (b). The rigid boundary is set to record reflected blast pressure histories, from which peak reflected overpressure and peak reflected impulse can be determined. The other two boundaries are set as outflow boundaries.



(a) 3D FE model



(b) Mapping 2D FE model

Fig. 2 FE model of explosive and air

2.2 Material model

The constitutive model *MAT_HIGH_EXPLSOIVE_BURN is utilized to model the mechanical properties of TNT. The equation of state *EOS_JWL defines the pressure as a function of the relative volume and initial energy per initial volume, such that

$$P = A \left(1 - \frac{\omega}{R_1 V} \right) e^{(-R_1 V)} + B \left(1 - \frac{\omega}{R_2 V} \right) e^{(-R_2 V)} + \frac{\omega}{V} E_0$$
 (1)

where A, B, R_1 , R_2 , and ω are constants; P is pressure; V is the relative volume;

 E_0 is the initial internal energy; and D is the detonation velocity. The material parameter of TNT is listed in Table 1 [40].

Table 1 TNT material parameter [40]

Density (kg/m³)	Detonation velocity (m/s)	C-J pressure (Pa)	A (Pa)	B (Pa)	R_I	R_2	ω	E_0 (J/m ³)
1630	6930	2.1e10	3.74e11	3.74e9	4.15	0.9	0.35	6e9

The constitutive model *MAT_NULL is used to model the mechanical properties of air. The polynomial EOS is linear in internal energy *E* per unit initial volume. The pressure used is given by:

206
$$P = C_0 + C_1 \mu + C_2 \mu^2 + C_3 \mu^3 + (C_4 + C_5 \mu + C_6 \mu^2) E$$
 (2)

where C_0 , C_1 , C_2 , C_3 , C_4 , C_5 and C_6 are constants and $\mu = \frac{\rho}{\rho_0} - 1$ with $\frac{\rho}{\rho_0}$ the ratio of current density to initial density. For gases which the gamma law equation of state applies, such as air, the above equation reduces to $P = (\gamma - 1) \frac{\rho}{\rho_0} E$ with γ the ratio of specific heats. The parameter of air is listed in Table 2, after Ref. [40].

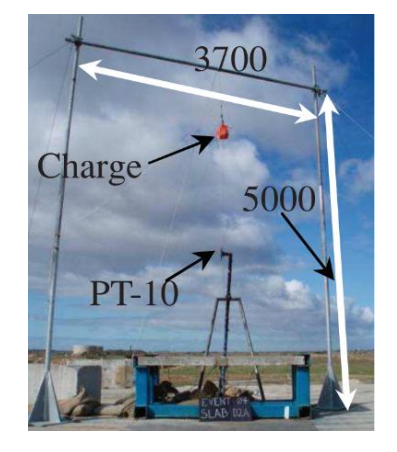
Table 2 Air material parameter [40]

Density (kg/m³)	Initial energy (J/m ³)	$C_0 - C_3$	C ₄	C ₅	C_6
1.225	2.5e5	0	0.4	0.4	0

2.3 Verification of numerical simulation

Wu et al. [41] conducted the blast tests on a 2000×2000×100 mm reinforced concrete slab to study the spatial and temporal distributions of reflected overpressure and impulse as a function of charge shape and orientation. The charges were suspended from a braced pipe frame as shown in Fig. 3 (a). Among those blast tests, three were performed using spherical charges, as listed in Table.3. Typical spherical charges are shown in Fig. 3 (b). The explosive was Composition B (a 60/40 RDX/TNT mixture with 1% added paraffin wax, detonation velocity of approximately 8,050 m/sec) that required a booster charge for detonation. The booster was located at the centre of the

charge. The UFC-3-340-02 design manual [2] computations assume a spherical charge and an equivalent mass of TNT equivalent (1.09 kg TNT per 1 kg of Composition B) to calculate scaled distance.





(a) Test instrument

(b) 2.5 kg spherical charge

Fig. 3 Blast test program [41]

Table.3 Blast test scheme of spherical charge [41]

Test	Standoff distance (m)	Scaled distance(m/kg ^{1/3})	Explosive mass (kg)	Charge shape	Equivalent TNT mass (kg)	Radius of TNT (mm)
14	2	3.12	0.24	Spherical charge	0.261	0.034
17	2	1.98	0.95	Spherical charge	1.036	0.053
19	2	1.43	2.5	Spherical charge	2.725	0.074

In order to verify the accuracy of ALE modelling approach, the numerical calculation results are validated using data recorded from the testing program above. Fig. 4 presents the predicted and measured reflected overpressure histories for test No.14, 17 and 19. It is observed that the magnitude and shape of time histories of the simulation results are in good agreement with those from the experiments [41].

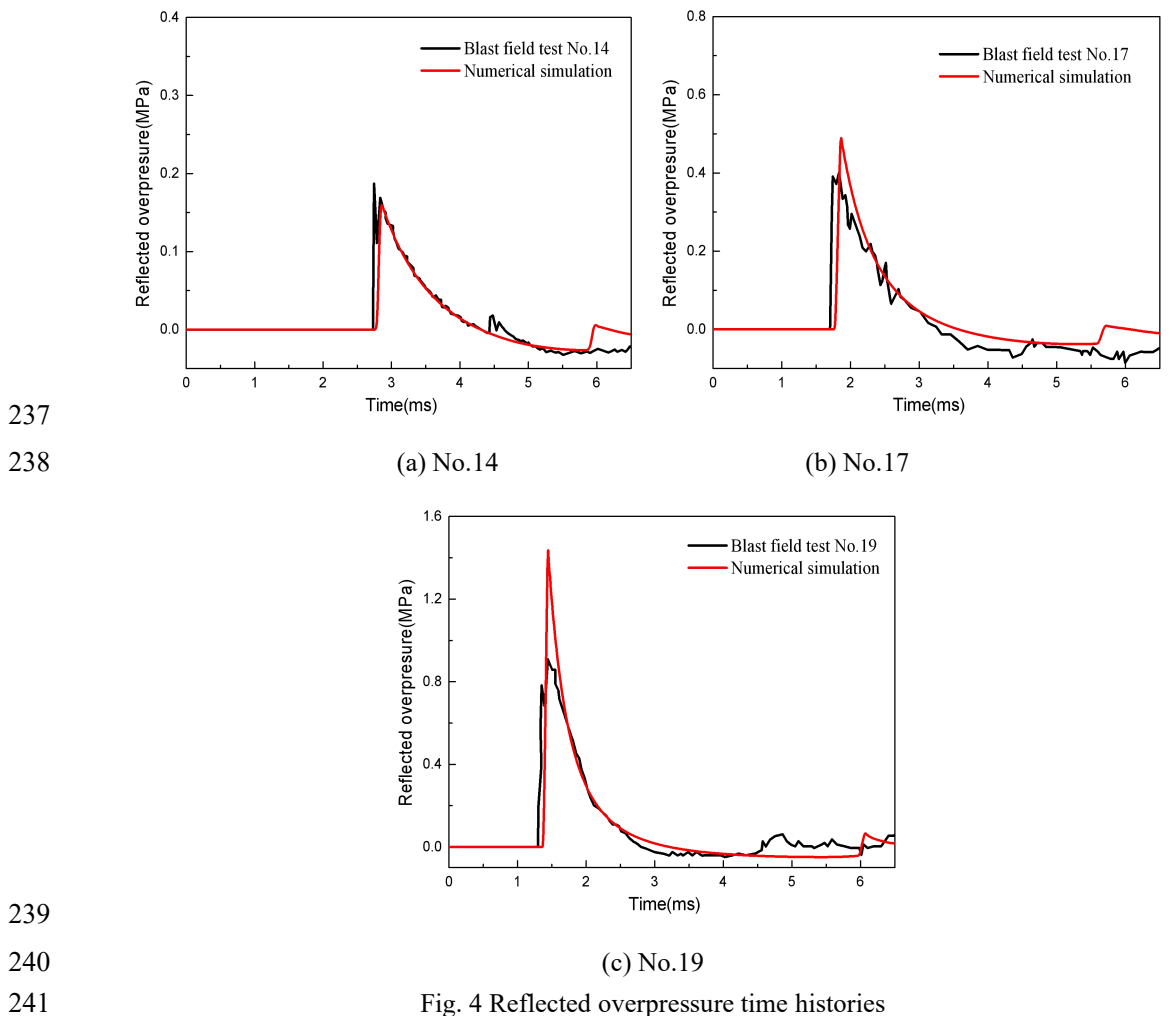


Fig. 4 Reflected overpressure time histories

242

243

244

245

246

247

248

249

250

251

252

253

254

Table 4 lists the comparison of blast parameter in the test and numerical simulation. In test No.14, the difference of time of positive phase duration, reflected peak overpressure and reflected impulse are 4.6%, 14.8% and 12.3%, respectively. In test No.17, the difference of time of positive phase duration, reflected peak overpressure and reflected impulse are 15.9%, 22.2% and 2.1%, respectively. In test No.19, the difference of time of positive phase duration, reflected peak overpressure and reflected impulse are 22.7%, 58.0% and 4.3%, respectively. Peak overpressure deviation in No.19 is higher compared with other parameter. In fact, the scaled distance in No.19 is 1.43 kg/m³, peak overpressure in the numerical simulation is 1.44 MPa, meanwhile, it is found from the report of UFC standard that the peak overpressure of TNT in free air is about 1.6 MPa. Numerical result coincide to UFC result well which demonstrates the accuracy of FE model parameters more advantageously although there is a large difference between numerical result and the blast experiment of Composition B. Whilst there are minor differences between other simulation and experimental results, it can be said that the model effectively predicts measured values of peak reflected overpressure, positive phase duration and reflected impulse and can be used with confidence to study the effects of uncertainties on blast load parameters.

Table 4 Comparison of blast load parameters

Blast load parameters	Numerical result	Experimental result	Error
Positive during time in No.14/ms	1.57	1.65	4.6%
Peak overpressure in No.14/Mpa	0.16	0.19	14.8%
Impulse in No.14/(Mpa·ms)	0.09	0.10	12.3%
Positive during time in No.17/ms	1.79	1.55	15.9%
Peak overpressure in No.17 /Mpa	0.49	0.40	22.2%
Impulse in No.17/(Mpa·ms)	0.25	0.25	2.1%
Positive during time in No.19/ms	1.84	1.50	22.7%
Peak overpressure in No.19 /Mpa	1.44	0.92	58.0%
Impulse in No.19/(Mpa·ms)	0.55	0.52	4.3%

3 PSL-Blast: Probabilistic statistic model of near-field blast loading

In order to consider the influence of scaled distance on the blast wave induced by fireball surface instabilities and stochastic detonator location, the variable of scaled distance Z is determined by fixing the TNT weight W and changing standoff distance R. Table 5 lists the detailed configuration of numerical simulation in the probabilistic statistic model of near-field blast loading. The number of 1-kg spherical explosive elements, of 5mm side length, is 4896.

Table 5 Parameter of spherical TNT

Standoff distance <i>R</i> (m)	TNT weight W (kg)	Scaled distance Z (m/kg $^{1/3}$)	Radius of spherical TNT (m)	Number of explosive elements
0.4	1.00	0.4	0.053	4896
0.6	1.00	0.6	0.053	4896
0.8	1.00	0.8	0.053	4896
1.0	1.00	1.0	0.053	4896
1.2	1.00	1.2	0.053	4896
2.0	1.00	2.0	0.053	4896
3.0	1.00	3.0	0.053	4896

3.1 Blast load parameters

In order to study the influence of fireball surface instability and detonator location on blast loads, it is necessary to first define the blast load parameters of interest. Fig. 5 shows a typical reflected overpressure time history at some arbitrary distance from a chemical explosive. It can be seen that overpressure near-instantaneously rises from atmospheric pressure, P_0 , to the overpressure, P_r , and subsequently decreasing exponentially to atmospheric pressure P_0 , over an interval known as the positive duration time t_0 . This period is considered to be critical for quantification of structural response and damage from an explosion, particularly in the extreme near-field. Afterwards, as the shock wave continues to propagate, the overpressure drops to negative pressure and then gradually returns to atmospheric pressure. Whilst the negative phase is critical for low-mass elements in the far-field [42], its contribution to net impulse in the near-field is negligible. Therefore, in this section, the peak overpressure and positive phase impulse of blast loads are chosen as blast load parameters to analyse the influence law of fireball surface instability and stochastic detonator location on blast loads.

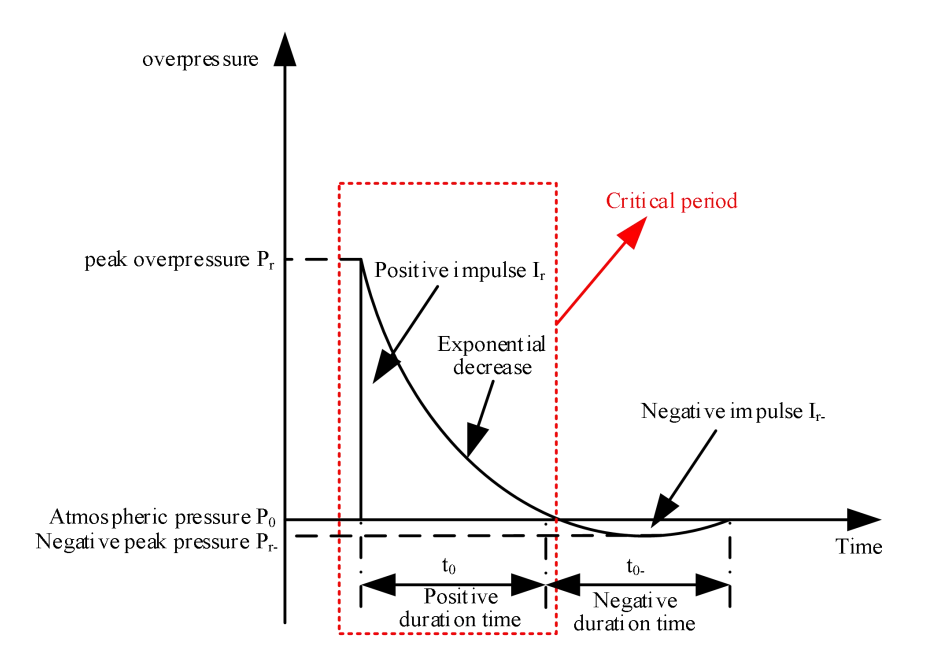


Fig. 5 Typical reflected overpressure time histories

300

301

302

303

304

305

306

307

308

309

310

311

312

313

314

315

316

317

3.2 Variability of blast load parameters induced by fireball surface instability

In order to characterise irregular features of fireball surface hydrodynamic instabilities, numerical simulations were performed with stochastic charge shape. In FE model, charge element is modelled and controlled by the two keywords in the LSDYNA, including MAT HIGH EXPLOSIVE BURN and EOS JWL. The important parameters for the charge are density, mass and detonation energy, which can mainly effect variation in the blast load, like the peak overpressure and impulse. It is known that density and mass are closely related to charge weight, and the unit of detonation energy is J/m³ or J/kg which is similarly related to charge weight. Therefore, in order to control the variable and investigated fireball instability effect under same scaled distance, it need to be guaranteed that the volume and weight of charge need to be kept constant to keep the density, mass and detonation energy constant. Additionally, the stochastic spatial distribution of blast wave from the stochastic oscillations at the edge of the fireball or fireball surface instability is not able to be described even if these parameters are randomized. Considering above reason, the stochastic charge shape with the same charge weight and charge volume is considered to describe the fireball instability and subsequent blast load parameter.

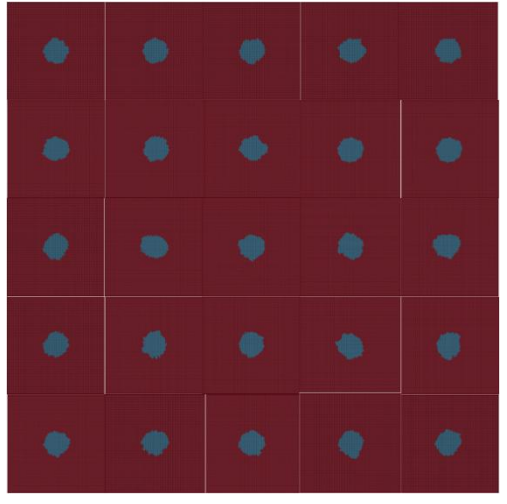
318	This section first proposes a new algorithm for generating charge elements with
319	stochastic shape. The charge is described to occupy a single volume in the domain,
320	without an internal 'hole'. The algorithm is therefore designed in order to prevent
321	such a hole from appearing, and is given by the following steps,

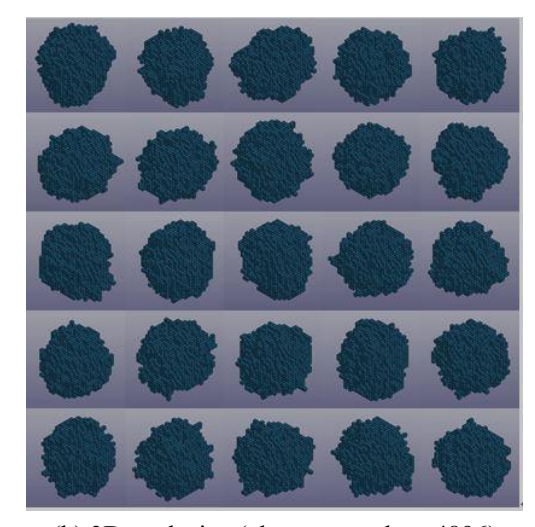
- 322 (a) Randomly choose a boundary location and add to the 'pool' of existing boundaries;
- 324 (b) Calculate the element bordered on the boundary and take away the unfilled selements among them;
- 326 (c) Randomly chose and fill in one of the elements above;
- 327 (d) After filling in the specified element in Step (c), determine whether all of 328 elements bordered on the specified element in Step (c) are filled in. If not, the 329 coordinate of the element is added in the boundary pool.
- 330 (e) Determine whether all of the bordered elements in Step (d) are filled, if all of 331 elements adjacent to the bordered element are filled *and* the bordered element is 332 in the boundary pool, the bordered element is removed from the boundary pool.
- 333 (f) Loop from Step (a) to Step (e) until the designated area and volume is generated.
 - Fig. 6 shows the 2D and 3D explosive with stochastic charge shape, with charge element numbers of 2000 and 4896 respectively, as defined through the aforementioned algorithm. It is observed that there exists no 'hole' in the internal area of the generated area and the proposed algorithm guarantees the stochastic characteristic of charge shape.

335

336

337





(a) 2D explosive (element number=2000)

(b) 3D explosive (element number=4896)

Fig. 6 Explosive element with the random charge shape

Fig. 7 shows the pressure contour with fireball surface instability characterized by the stochastic charge shape under the scaled distance of Z =1.0 m/kg^{1/3}. As shown in Fig. 7 (c), it is observed from shock wave shape that the spatial distribution of shock wave with the stochastic charge shape is non-uniform around the charge, which appears visually similar to fireball surface instabilities observed in high speed video footage of near-field explosions [26]. The raw high-speed video still or the edge detection image only show that the edge of the fireball is a stochastic process. Whether it is the stochastic oscillation at the edge of the fireball or fireball surface instability, they finally result in the unstable shape of blast wave. FE analysis itself is not be able to reproduce the unstable shape of blast wave induced stochastic oscillations at the edge of the fireball. This paper proposes a stochastic algorithm and try to reproduce unstable blast wave shape induced by the stochastic oscillation at the edge of the fireball or fireball surface instability. Observed from Figure 7(c), this stochastic algorithm can well reflect the stochastic blast wave shape induced by the stochastic oscillation at the edge of the fireball or fireball surface instability.

Therefore, this approach can effectively emulate the stochastic features of a shock wave induced by fireball surface instabilities. In addition, the pressure fringe plot in Fig. 7 (c) shows that a stochastic charge shape will not only affect the spatial distribution of a blast but will also influence the distribution of blast load parameters,

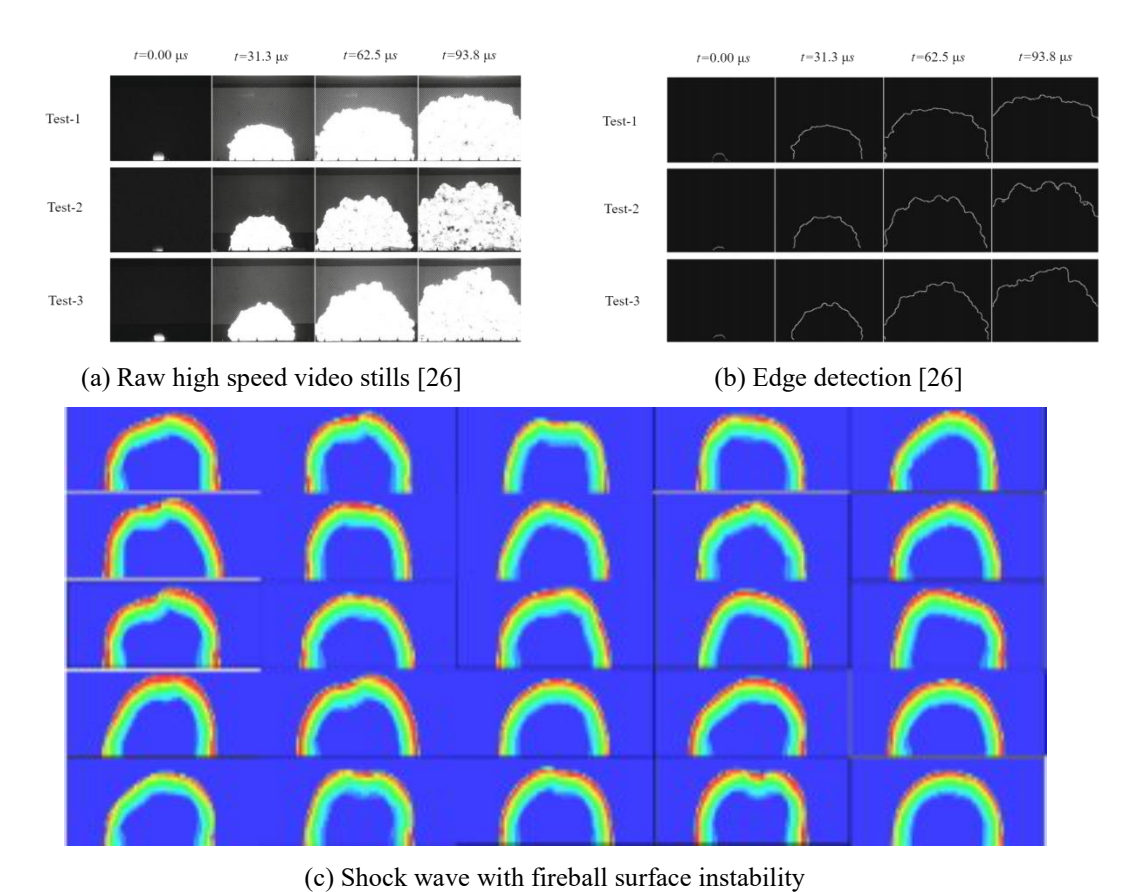


Fig. 7 Pressure contour with fireball surface instability (Z=1.0 m/kg^{1/3})

In order to analyse the uncertainty of blast loads induced by fireball surface instability, a dimensionless fireball shape coefficient is proposed, which is defined by the ratio of blast load parameters induced by the instable fireball surface calculated from a numerical model with stochastic charge shape to that induced by the ideal spherical fireball surface calculated from a numerical model with ideal spherical charge shape. The detailed expression is described as follows,

Fireball shape coefficient
$$(P_{\text{CSE}} \text{ and } I_{\text{CSE}}) = \frac{Value_{\text{instable fireball surface}}}{Value_{\text{ideal spherical fireball surface}}}$$
 (3)

where, P_{CSE} and I_{CSE} represent the ratio of peak overpressure and positive duration impulse induced by the fireball surface instability to that induced by the ideal spherical shock wave, respectively.

Fig. 8 shows the statistics and relationship for P_{CSE} and I_{CSE} against scaled distance Z. It is observed that the envelope of P_{CSE} and I_{CSE} becomes narrower with

increasing scaled distance. When scaled distance is 0.4 m/kg^{1/3}, the peak overpressure induced by a random charge shape is up to 1.9 times higher than that induced by a spherical charge, and the impulse induced by a random charge shape is up to 1.3 times higher.

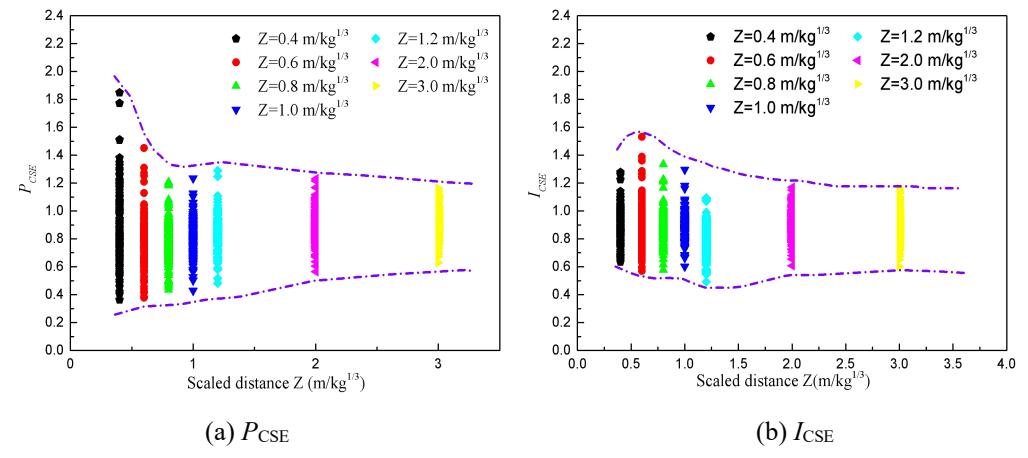
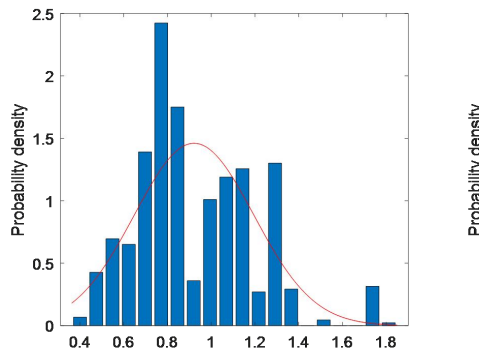
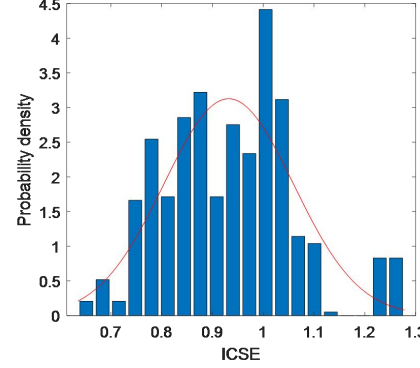


Fig. 8 Data statistics of charge shape coefficient (Number=600)

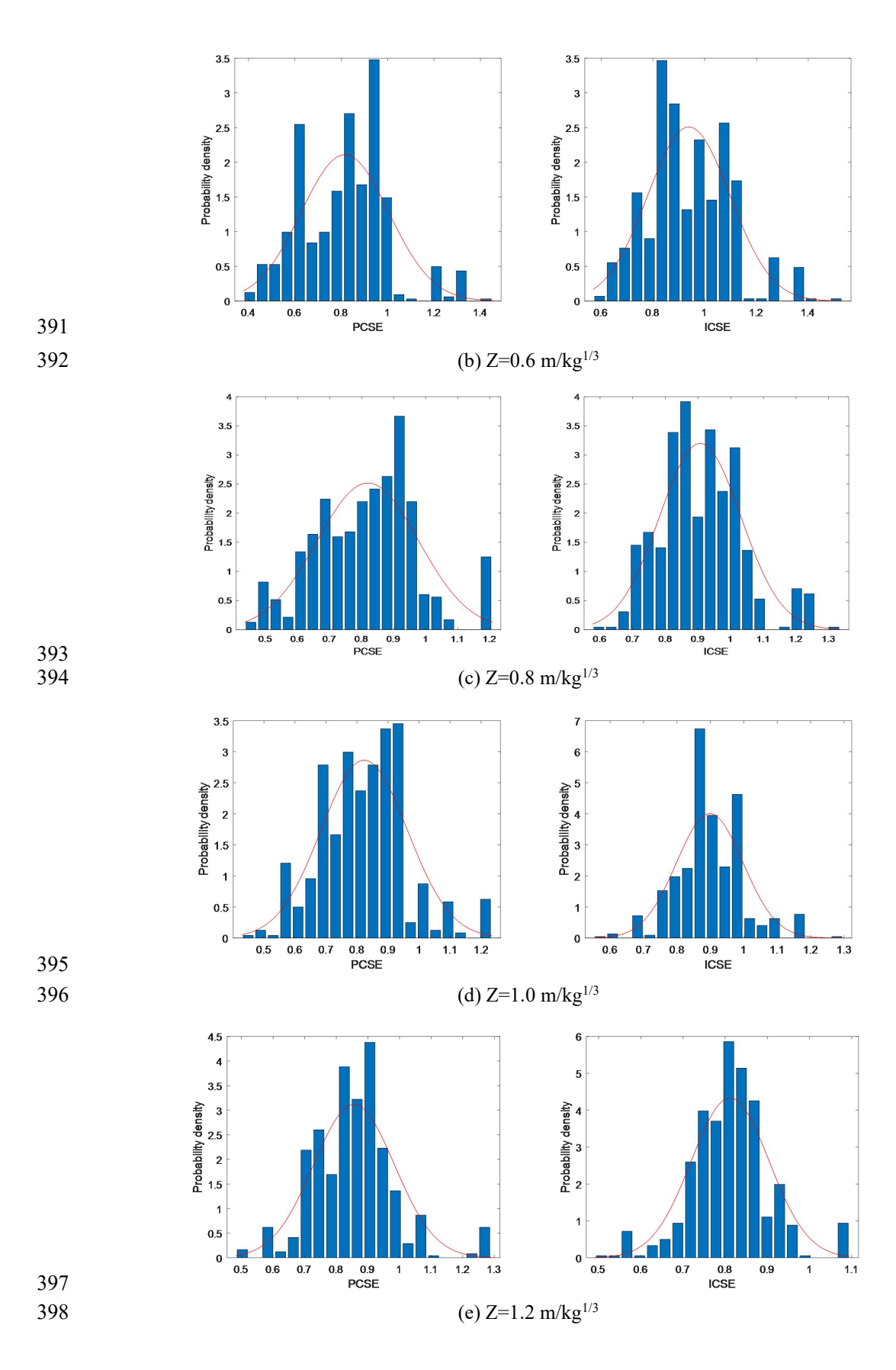
Fig. 9 shows the discrete distribution of P_{CSE} and I_{CSE} , which can both be approximated by a normal distribution, $N(\delta, \sigma^2)$, where δ is mean and σ and σ^2 are standard deviation and variance, respectively.



PCSE



(a) $Z=0.4 \text{ m/kg}^{1/3}$



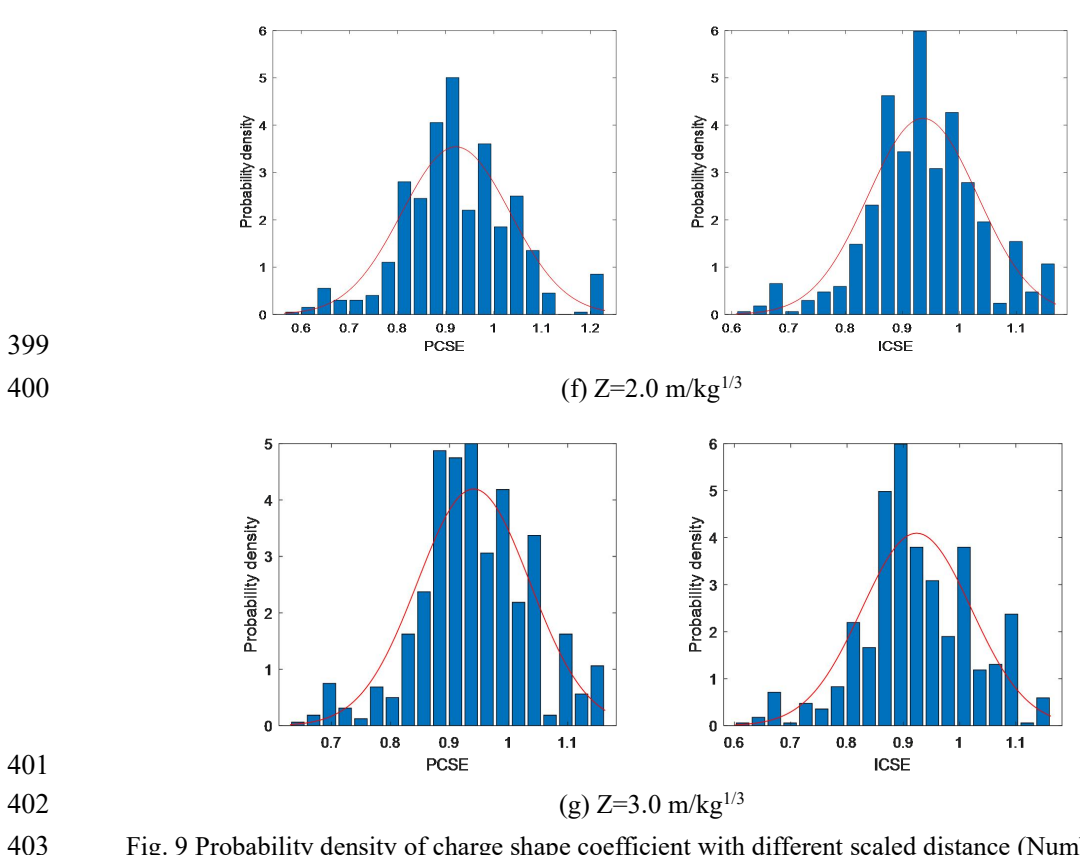


Fig. 9 Probability density of charge shape coefficient with different scaled distance (Number=600)

Commonly used hypothesis testing methods include S-W and K-S tests. However, it should be noted that when the sample size is small, these tests are not sufficiently sensitive, and when the sample size is large, the tests are too sensitive. Therefore, due to the large number of samples in this paper, it is necessary to combine results from the histograms with a Q-Q graph to more robustly analyse the distribution of data. The Q-Q graph reflects the coincidence degree between the actual distribution of variables and the theoretical distribution, and can be used to check whether the data obey a certain distribution type. If the data follows a certain distribution, the data points should coincide substantially with the theoretical line. Fig. 10 shows the Q-Q graph of charge shape coefficient based on standard normal samples. It can be seen that the data points on the Q-Q graph are distributed on a straight line, which effectively coincides with the theoretical line, indicating that the data approximately follows a normal distribution.

404

405

406

407

408

409

410

411

412

413

414

415

416

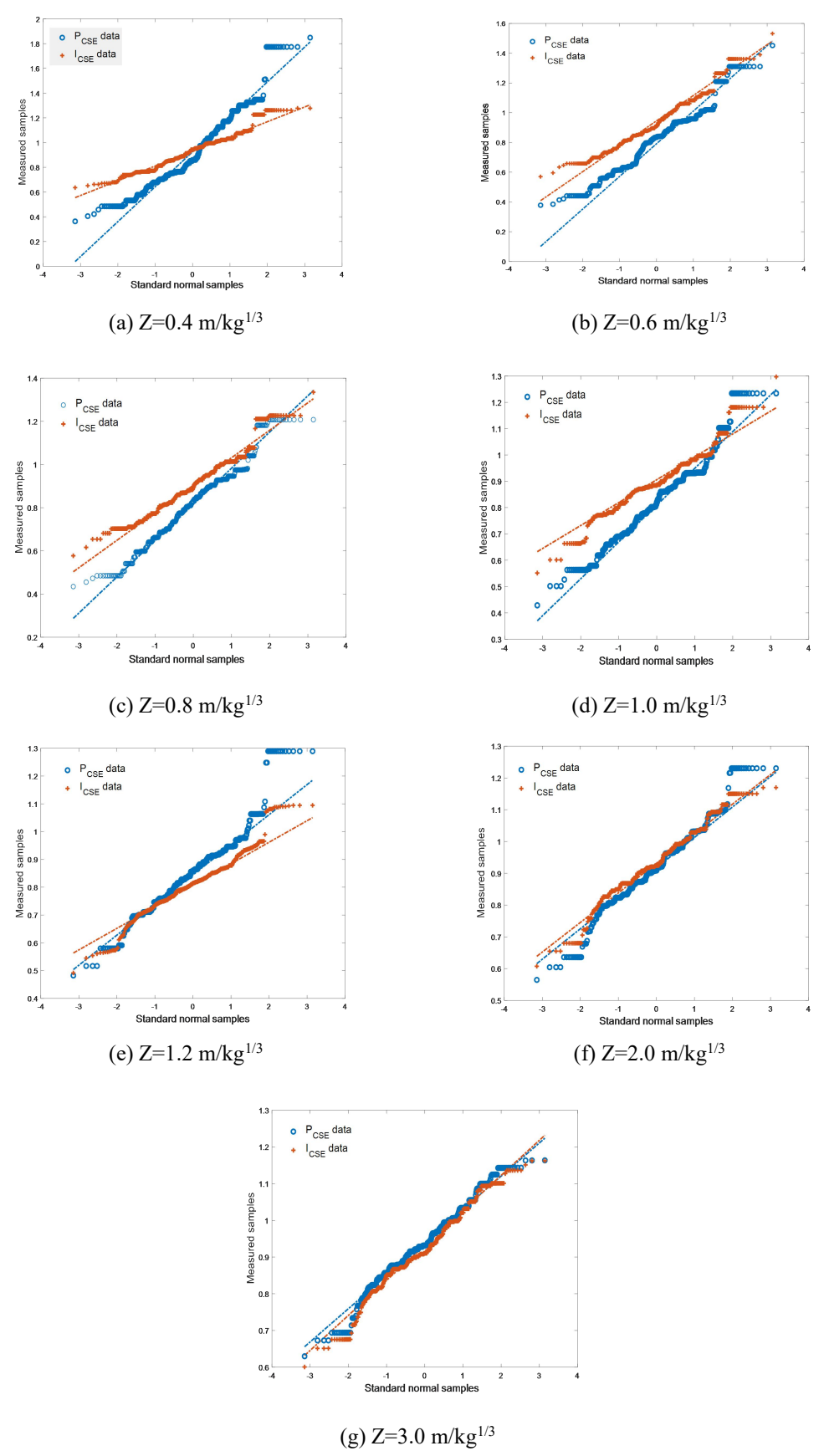


Fig. 10 Q-Q plot of charge shape coefficient

The variability of P_{CSE} and I_{CSE} is fitted as a function of scaled distance, Z, as shown in Fig. 11 and Fig. 12. It is observed that the mean of P_{CSE} and I_{CSE} is smaller than, but tends towards 1.0, which suggests that the net effect of a stochastic charge shape is a slight reduction in blast loading. It is observed from Fig. 12 that there exists a seemingly greater variability at lower scaled distance Z for the peak overpressure and impulse, which is in agreement with common observations of a decrease in variability of blast loading as the situation approaches the far-field. The lines of best fit for P_{CSE} and I_{CSE} are listed in Table 6.

429

421

422

423

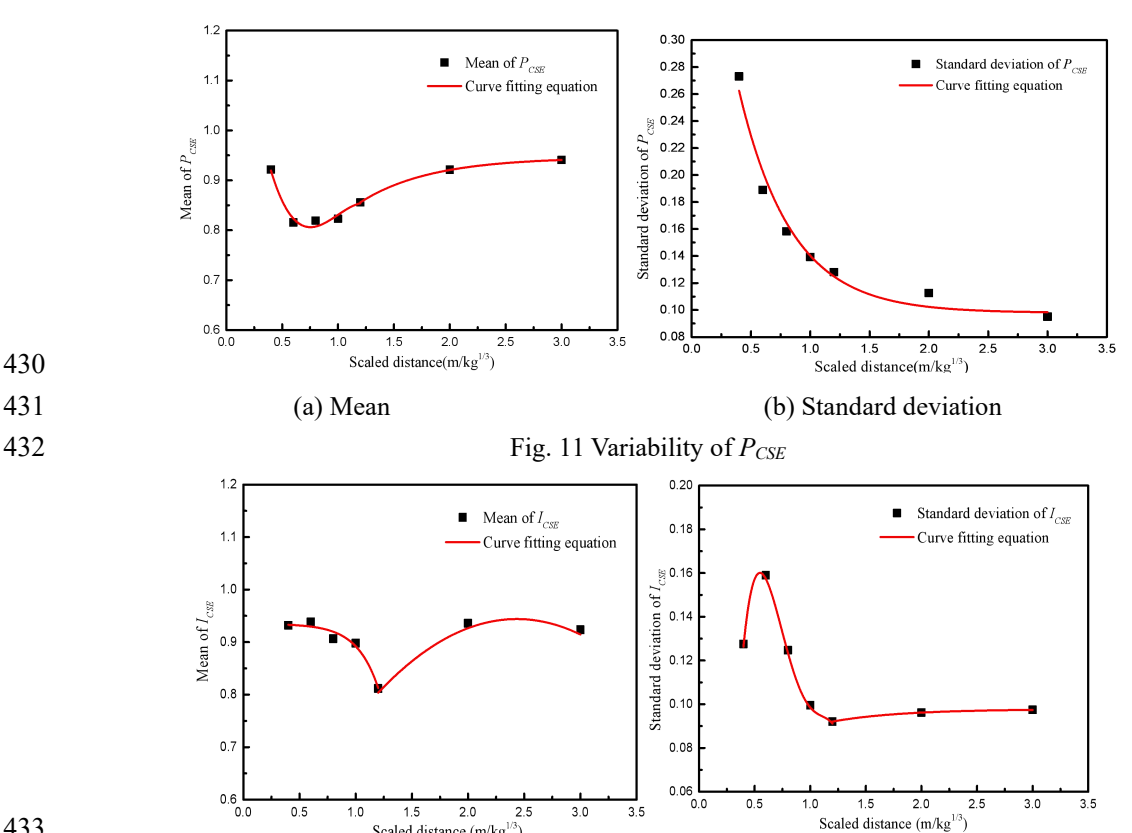
424

425

426

427

428



3.0

2.0

Scaled distance (m/kg1/3)

(a) Mean

433 434 435

Fig. 12 Variability of I_{CSE}

(b) Standard deviation

3.5

436 437

438

439

440

Parameter	Mean	Mean Standard deviation	
P_{CSE}	1.5121 - 2.3494 × Z + 2.5054 × Z^2 - 0.8372 × Z^3 , $Z \le 1.2 \text{ m/kg}^{1/3}$ ($R^2 = 96.5\%$) 0.9459 - 0.6081 × $e^{\frac{Z}{0.6281}}$, $Z > 1.2 \text{ m/kg}^{1/3}$	$0.0979 + 0.4066 \times e^{-2.2610 \times Z}$ $(R^2 = 98.6\%)$	Normal
I_{CSE}	$(R^2=99.9\%)$ $0.9349 - 2.2799 \times 10^{-4} \times e^{-\frac{Z}{-0.1910}}, Z \le 1.2$ $m/kg^{1/3} (R^2=97.1\%)$	$-0.7563 + 4.6839 \times Z -$ $8.4547 \times Z^2 + 6.3372 \times Z^3 -$ $1.7116 \times Z^4, Z \le 1.2 \text{ m/kg}^{1/3}$ $(R^2 = 99.9\%)$	Normal
	$0.3981 + 04485 \times Z - 0.0921 \times Z^2, Z > 1.2$ m/kg ^{1/3} ($R^2 = 99.3\%$)	$0.0978 - 0.0390 \times e^{-\frac{Z}{0.6215}},$ Z>1.2 m/kg ^{1/3} (R ² =99.9%)	

3.3 Variability of blast load parameters induced by stochastic detonator location

In order to investigate the effect of stochastic detonator location on the blast wave, an additional numerical study was undertaken, whereby the 3D coordinates of the detonator location were randomly chosen. In the case of detonator locations lying outside of the explosive charge, these were rejected and a new set of coordinates were selected.

Fig. 13 shows the FE model of 1 kg spherical charge with stochastic detonator location. The yellow pentagram represents the detonation point location in the internal spherical charge. The distance between detonator location and charge centre is defined as $D= \operatorname{sqrt}[x^2 + y^2 + z^2]$, and is indicated in each sub-figure.

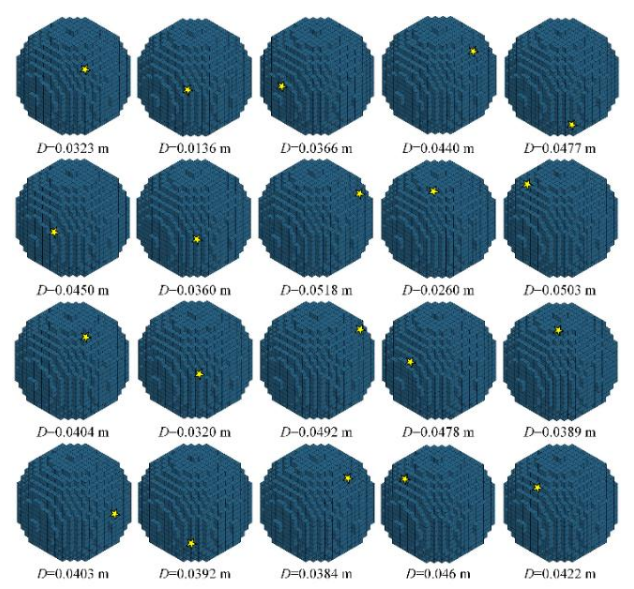


Fig. 13 1 kg TNT sphere with stochastic detonator location

As previously, in order to analyse the uncertainty of near-field blast loads induced by the stochastic detonator location, a dimensionless detonator location coefficient is proposed. This is given by the ratio of the blast load parameters induced by the stochastic detonator location to that induced by the centre-initiated detonation. The detailed expression is given as,

Detonator location coefficient (P_{DLE} and I_{DLE}) = $\frac{Value_{stochastic\ detonator\ location}}{Value_{centre-initiated\ detonation}}$ (4) where, P_{DLE} and I_{DLE} represents the ratio of peak overpressure and impulse induced by the stochastic detonator location to that induced by the centre-initiated detonation, respectively.

Fig. 14 shows the statistics and relationship of P_{DLE} and I_{DLE} against scaled distance. It is observed that the envelope of P_{DLE} becomes narrower with increasing scaled distance, which again supports direct observation of blast parameter variability, and is consistent with previous findings in this article. Whilst the relationship between the envelope of I_{DLE} and scaled distance is unclear, both parameters are centred around a mean value of approximately 1.0, suggesting that the net effect on global blast loading is negligible. Considering the results locally, however, when the scaled distance is 0.4 m/kg^{1/3}, the peak overpressure induced by the stochastic detonator location is up to 1.4 times higher than that induced by the centre-initiated detonation, and the impulse induced by the stochastic detonator location is up to 1.2 times higher than that induced by the fireball surface instability, the difference induced by the detonator location is clearly smaller.

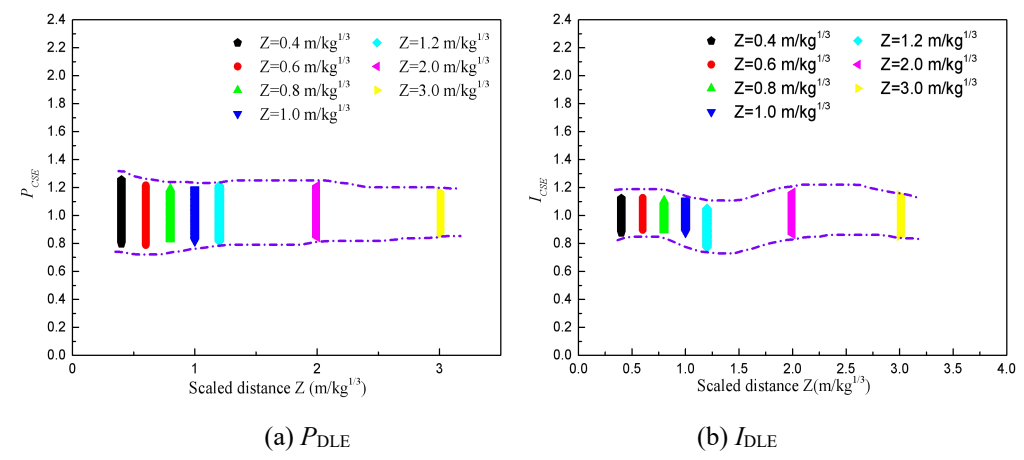
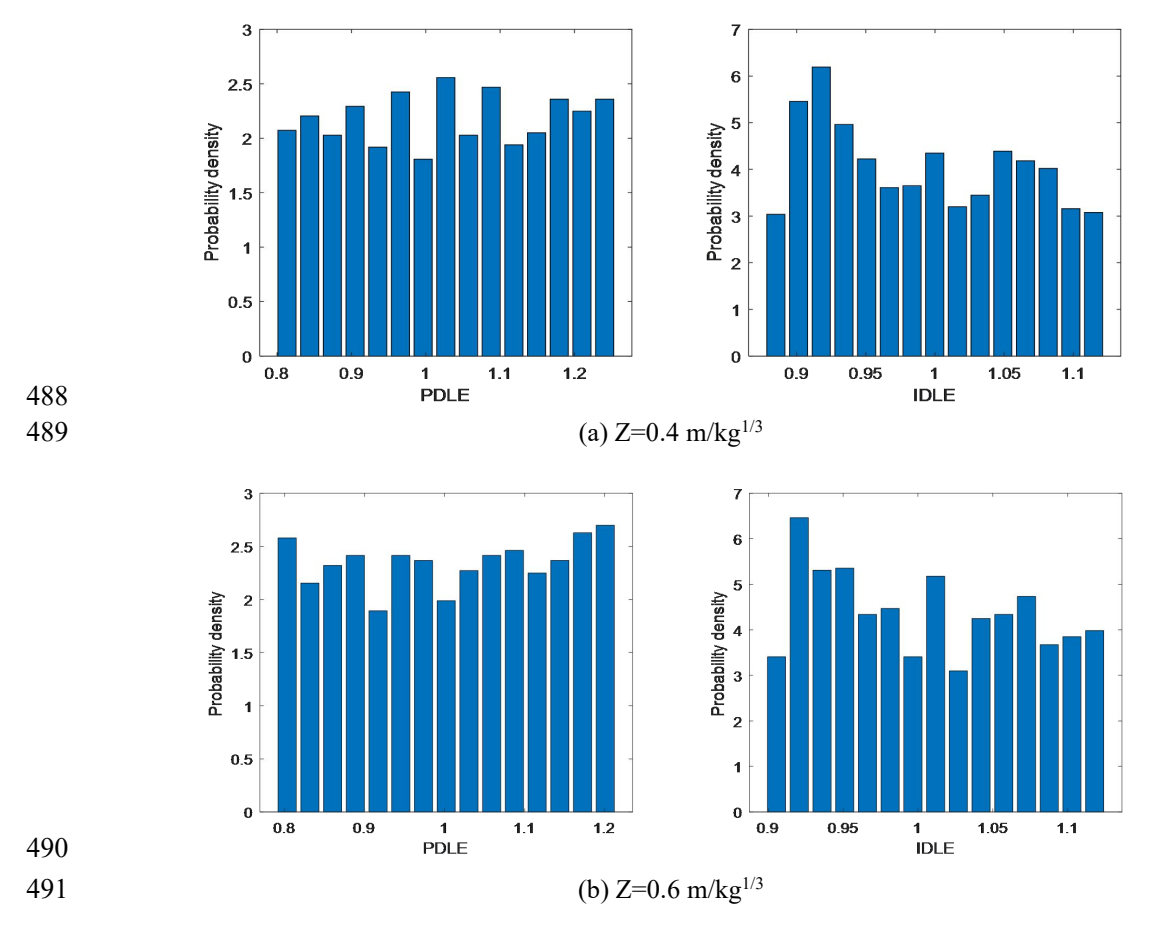
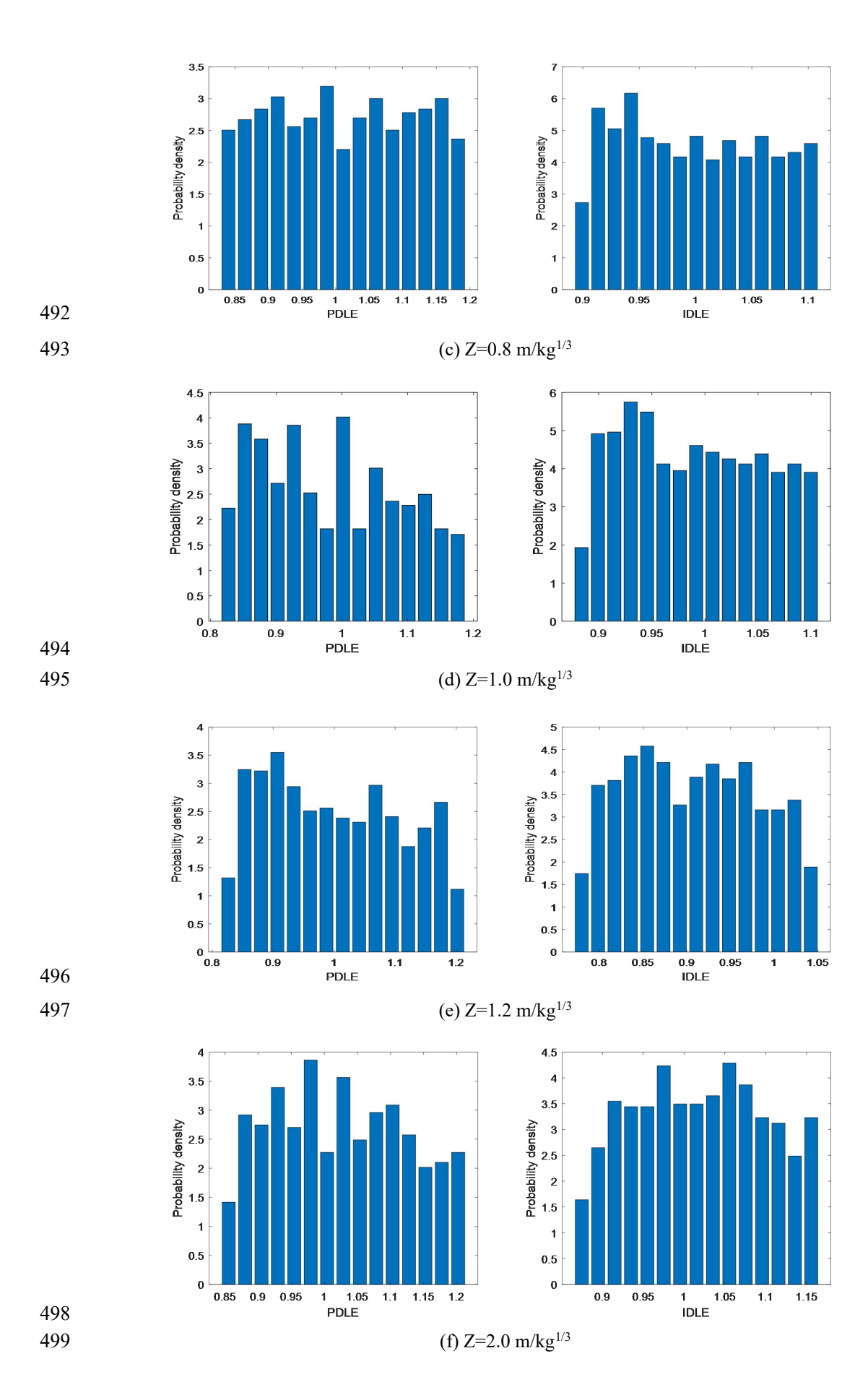


Fig. 14 Data statistics for the stochastic detonator location (Number=1500)

Fig. 15 shows the approximate distribution of P_{DLE} and I_{DLE} , which all appear to be approximately uniformly distributed. The uniform distribution is determined according to two parameters, minimum value a and maximum value b, given as U(a, b).





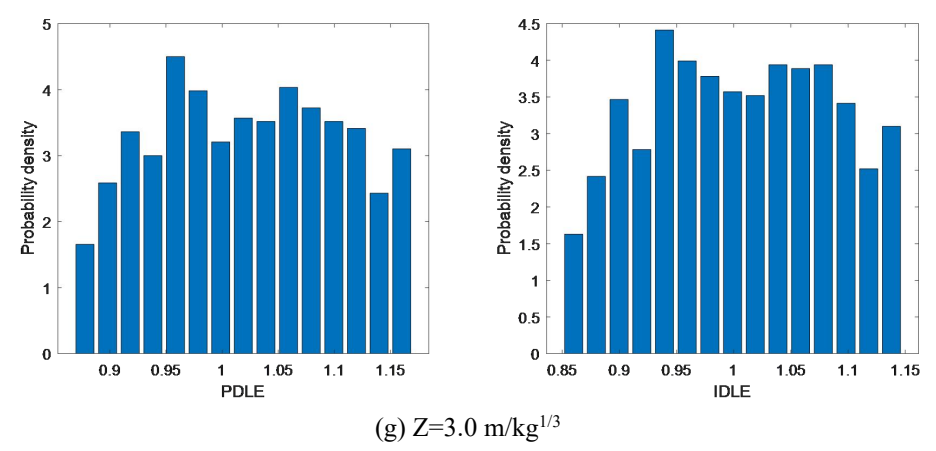
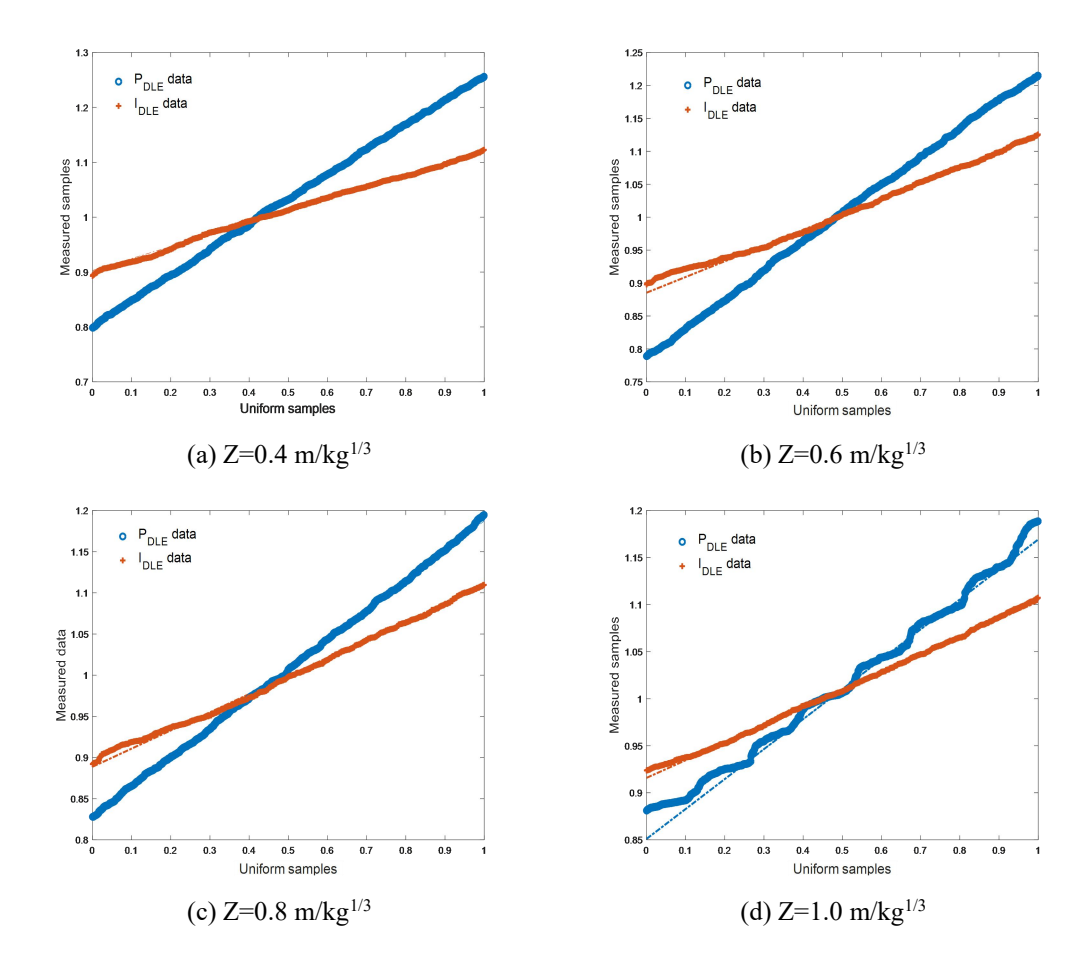


Fig. 15 Probability density of stochastic detonator location (Number=1500)

Fig. 16 shows the Q-Q graph of the stochastic detonator coefficient based on uniformly distributed samples. It can be seen that the data points on the Q-Q diagram are distributed on a straight line, which coincides with the theoretical line, indicating that it approximately follows the uniform distribution.



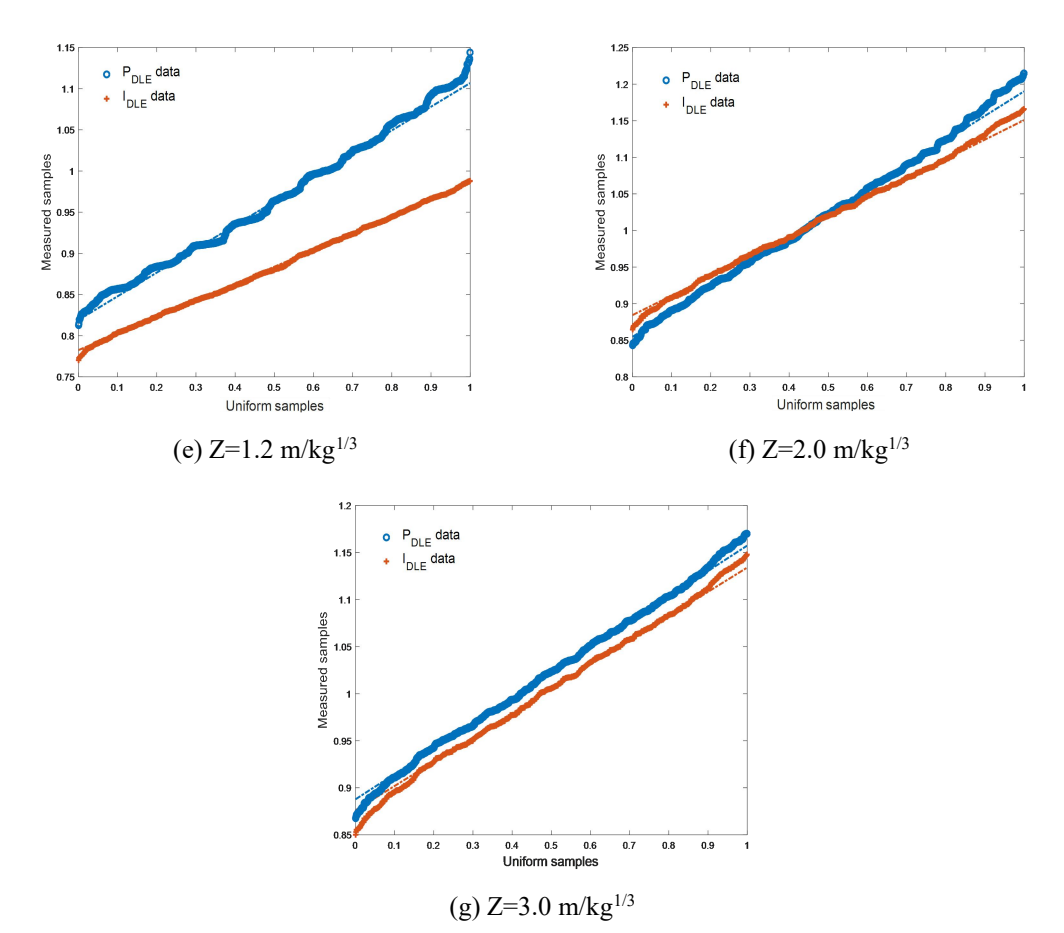


Fig. 16 Q-Q plot of detonator location coefficient

The variability of $P_{\rm DLE}$ and $I_{\rm DLE}$ is described and fitted as a function of scaled distance, Z, as shown in Fig. 17 and Fig. 18. It is observed that the parameters a and b can be approximated by two segmented curves. When the scaled distance is less than 1.2 m/kg^{1/3}, the parameters a and b are best fitted by a polynomial for both pressure and impulse; whereas when the scaled distance is more than 1.2 m/kg^{1/3}, the parameters a and b are best fitted by the polynomial for pressure and an exponential function for impulse. The detailed fitting expressions are listed in Table 7. Firstly, a and b value depend on the statistic of data calculated by much numerical simulation. The data is real and reliable. Furthermore, it can be seen from envelope of Figure 14 that blast variability induced by the stochastic detonator location is relatively small. It can be found that there is a very small difference of value a from the range 1.0 to 1.3 in the y-axis in Figure 18 (a), and the same goes for value b from the range 0.76 to 0.90 although a and b are lowest under the scaled distance of 1.2. It is possible that

data rule is not obvious in this very small difference. 524

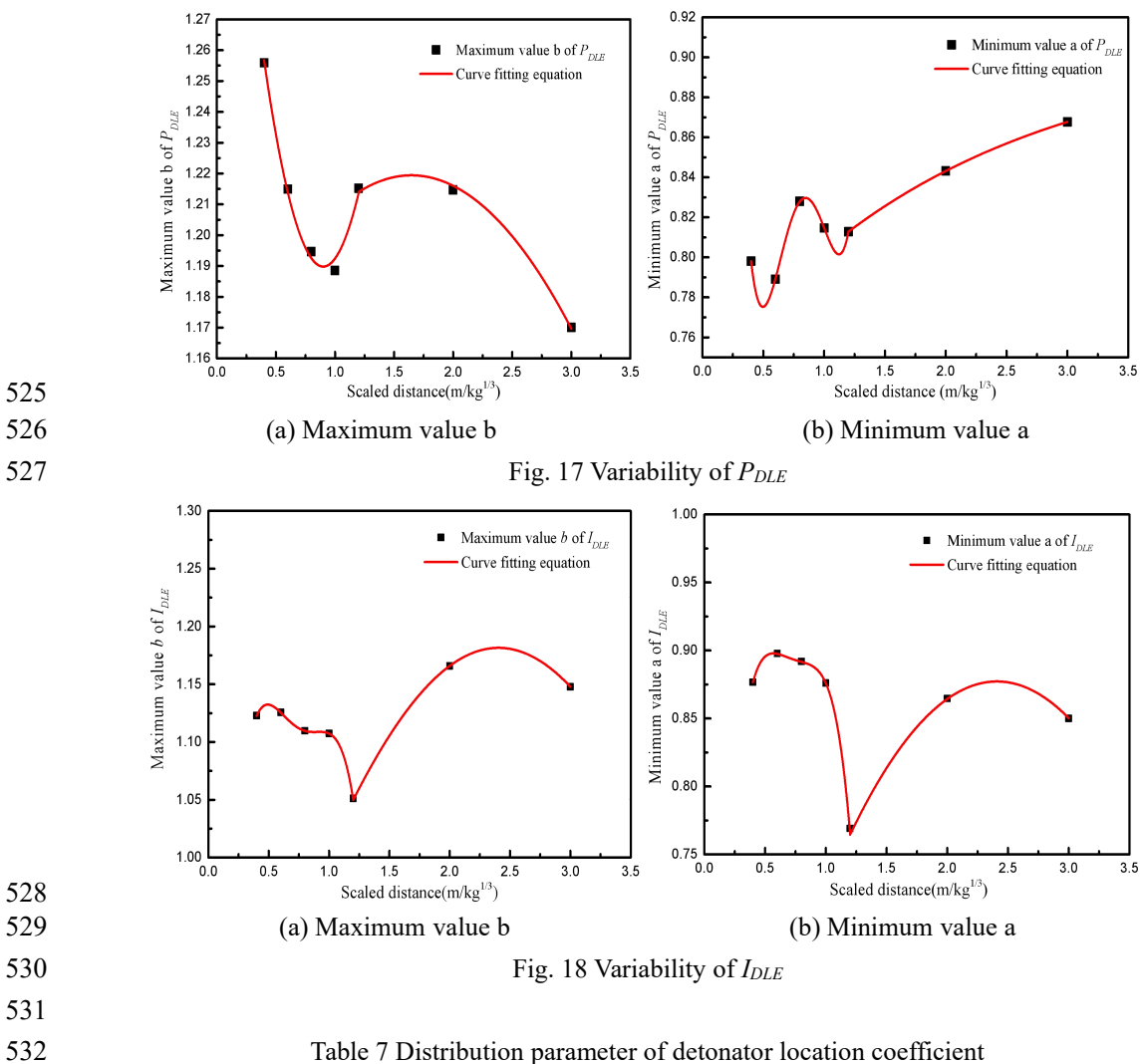


Table 7 Distribution parameter of detonator location coefficient

Paramete	Maximum value b Minimum value a		Distributio
r			n
P_{DLE}	1.4063 - 0.4806 × Z + 0.2667 × Z^2 , $Z \le 1.2 \text{ m/kg}^{1/3} (R^2 = 99.2\%)$	$2.1604 - 7.9586 \times Z + 16.2426 \times Z^{2} - $ $13.8351 \times Z^{3} + 4.2054 \times Z^{4}, Z \le 1.2$ $m/kg^{1/3}$ $(R^{2}=99.9\%)$	Uniform
	1.1458 + 0.0894 × Z - 0.0271 × Z^2 , Z >1.2 m/kg ^{1/3} (R^2 =99.7%)	$0.9069 - 0.1688 \times e^{-\frac{Z}{2.0567}}, Z > 1.2 \text{ m/kg}^{1/3}$ $(R^2 = 99.9\%)$	
I_{DEL}	$0.4307 + 4.1631 \times Z - 8.8591 \times Z^2 +$ $7.9849 \times Z^3 - 2.6123 \times Z^4, Z \le 1.2$ $m/kg^{1/3} (R^2 = 99.9\%)$	$0.1741 + 4.0942 \times Z - 8.5462 \times Z^{2} +$ $7.8192 \times Z^{3} - 2.6655 \times Z^{4}, Z \le 1.2$ $m/kg^{1/3}$ $(R^{2}=99.9\%)$	Uniform
	$e^{-0.3041+0.3916\times Z-0.0814\times Z^2}$, $Z>1.2$ m/kg ^{1/3} ($R^2=99.9\%$)	$0.4298 + 0.3715 \times Z - 0.0771 \times Z^2,$ $Z > 1.2 \text{ m/kg}^{1/3} (R^2 = 99.8\%)$	

4 Reliability design of near-field blast loads based on PSL-Blast

Reliability level and safety factor are defined with reference to Fig. 19. The safety factor is labelled as λ , which is consistent with the terminology in the UFC standard. The nominal load obtained from UFC standard is multiplied by the safety factor λ to ensure that the actual load is equal to the value of blast load with a certain reliability level. For example, a safety factor greater than 1 increases nominal loads resulting in more conservative structural designs.

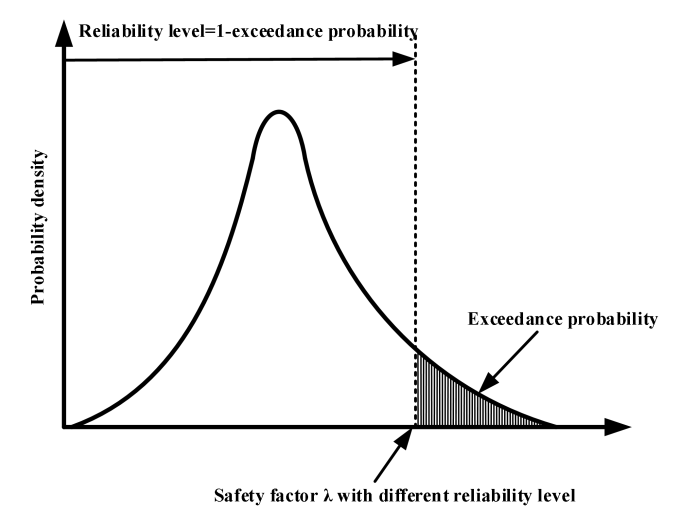


Fig. 19 Reliability-based load factor for a reliability level

4.1 Computational procedure for PSL-Blast

Table 6 and Table 7 list the distribution parameters for the probabilistic model of near-field blast loads. The critical input parameter in *PSL-Blast* includes the fireball surface instability and stochastic detonator location. This paper focuses on the variability from the internal part of charge more dedicatedly, especially close-in blast. The probabilistic model of fireball surface instability and internal detonator location is considered and established from the aspect of the blast mechanism for generating blast load uncertainty because some high speed videos show the stochastic oscillations at the edge of the fireball or fireball surface instability. Other variables such as moisture content, wind speed, and wind direction might impact the fireball surface instability. However, they were not included in this study due to numerical modeling

limitations.

555

556

557

558

559

560

561

562

563

564

565

566

567

A significant issue regarding model error relates to the possibility of a correlation between variables. The estimation of correlation coefficients shows little or no correlation. However, a moderate relationship is observed between fireball surface instability and stochastic detonator location. It is clear that there is reasonable statistical independence between each model error data, as such, blast load variability of fireball surface instability and stochastic detonator location may be assumed as statistically independent. If more appropriate comprehensive data sets are available then this can be used to update the calculations herein. What is important herein is the methodology of characterizing various sources of variability and uncertainty in the development of a probabilistic blast loading model. Furthermore, Monte-Carlo simulation is used as the computational tool. Each simulation of *PSL-Blast* run consists of the following computational steps:

- 568 (a) Randomly generate variables;
- 569 (b) Infer explosive mass (W) and stand-off (R);
- 570 (c) Calculate scaled distance (Z);
- (d) Calculate peak overpressure P_{model} and impulse I_{model} from blast loading model [2],
- as shown in Fig. 20;
- 573 (e) Correct P_{model} and I_{model} with the fireball shape coefficient P_{CSE} and I_{CSE} ;
- 574 (f) Correct P_{model} and I_{model} with the detonator location coefficient P_{DLE} and I_{DLE} ;
- After many simulations the probability distributions of P_r and I_r can be inferred.

576

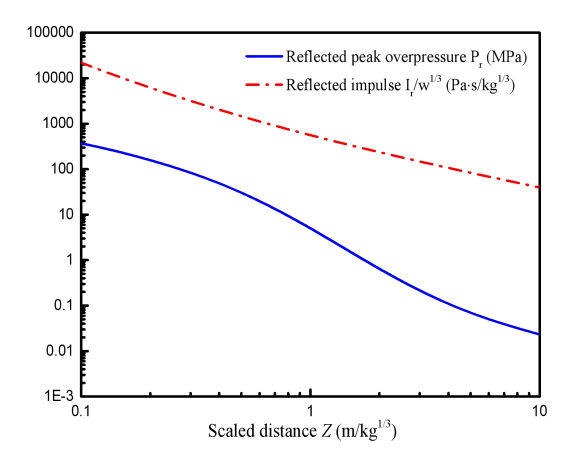


Fig. 20 Blast load parameters of spherical TNT in free air explosion [2]

4.2 Probabilistic analysis of blast parameter from the experiment

In order to verify the applicability of the probabilistic statistical model of blast loads, probabilistic analysis of blast load parameters from blast test of top-end-initiated spherical TNT and ConWep is carried out to estimate the exceedance probability of peak overpressure and impulse.

4.2.1 Blast test of top-end-initiated spherical TNT [6]

The blast load parameters measured by Shi et al. [6] were utilized to analyse the exceedance probability through the computational procedure of *PSL-Blast*. Fig. 21 shows the overall setup of the blast test. A 1500mm×1200mm×25mm steel plate was tightly bolted to a firm steel frame and five reflected pressure sensors were fixed on the steel plate. A steel sleeve was screwed into the pre-drilled hole of the steel plate into which the sensor was embedded appropriately. The pressure-receiving faces of the sensors and the steel plate were strictly coplanar to make sure that accurate measurement results were obtained. The charge was located by adjusting the length of the string bag and the hook. Before detonating, the location of the charge was checked to ensure it was within 2 mm tolerance. Testing point P2 is directly below the explosive, i.e., angle of incidence $\theta = 0^{o}$. The distance between the explosive center and the steel plate was 0.8m.

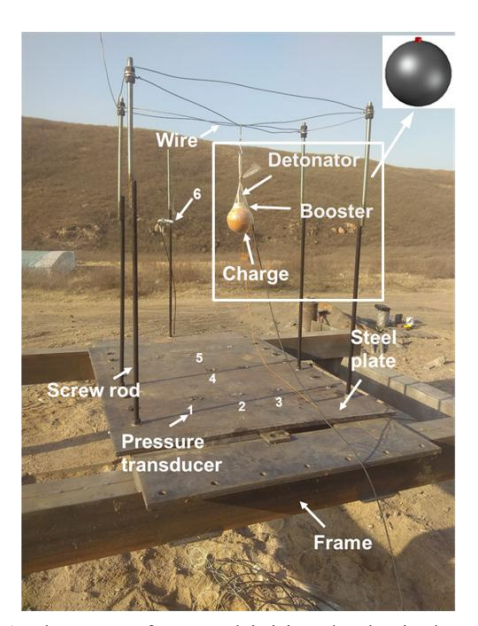


Fig. 21 Blast test of top-end-initiated spherical TNT [6]

The detailed test scheme and measured results are listed in Table 8. There are some degrees of scatter in peak overpressure and impulse under the same blast condition. Additionally, peak overpressure and impulse from blast tests of top-end-initiated spherical TNT are slightly larger than that of UFC design manual, which demonstrates that detonator location has a slight influence on the blast load parameters under the near-field explosion.

Table 8 Summary of experimental data from Shi et al. [6]

Test	Scaled	Equivalent	Experimental result		UFC design manual	
No.	distance(m/kg ^{1/3})	TNT mass	$P_r(MPa)$	I _r (MPa·ms)	$P_r(MPa)$	I _r (MPa·ms)
		(kg)				
S1	0.8	1.0	13.66	0.84	9.40	0.75
S2	0.8	1.0	10.53	0.66	9.40	0.75
S3	0.8	1.0	11.36	0.68	9.40	0.75

Fig. 22 and Fig. 23 show the probability distributions of P_r and I_r (for 500,000 simulations) under three test conditions of S1, S2 and S3, respectively. It is observed that the probability that the explosive load exceeds the experimental value under three test conditions of S1, S2 and S3 is 1%, 5% and 2% for P_r , respectively. The probability that the explosive load exceeds the experimental value under the three test conditions of S1, S2 and S3 is 6%, 57% and 49% for I_r , respectively. It is found from the test data and probability analysis that the exceedance probabilities of peak overpressure and impulse under the three same working conditions are quite different, indicating that there is a large uncertainty under near field blast loads.

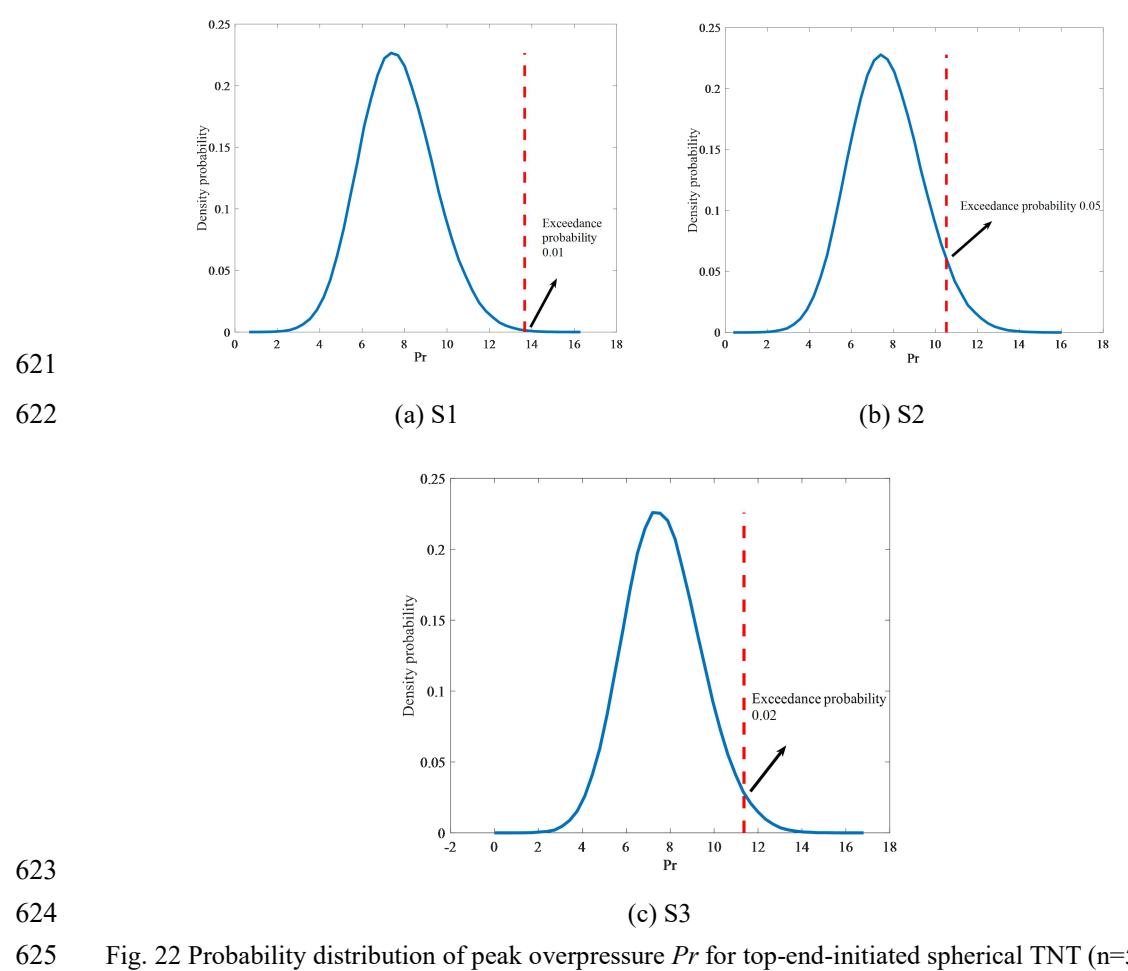
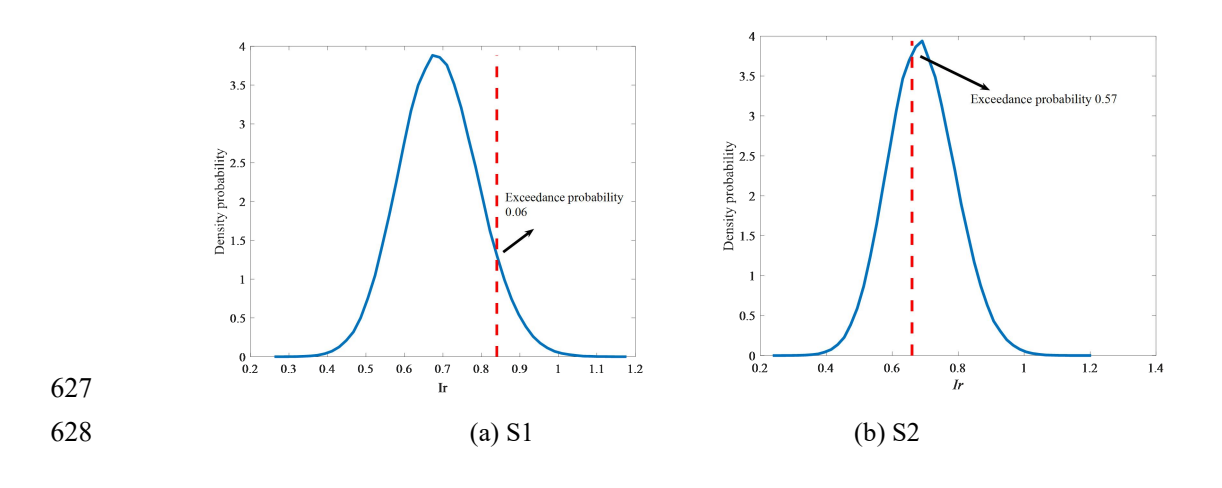


Fig. 22 Probability distribution of peak overpressure Pr for top-end-initiated spherical TNT (n=500000)



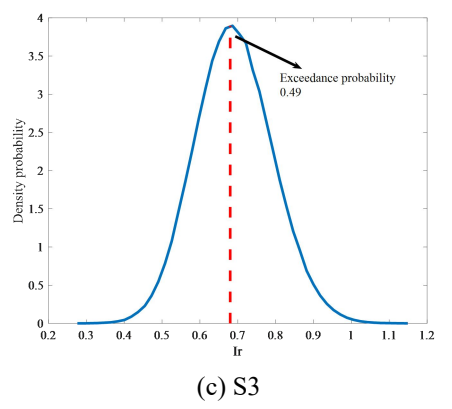


Fig. 23 Probability distribution of impulse *Ir* for top-end-initiated spherical TNT (n=500000)

4.2.2 Predictive computer code ConWep

The blast load parameters calculated by ConWep [3] are used to analyze the exceedance probability of P_r and I_r under PSL-Blast. Table 9 lists the blast load parameters under two chosen scaled distances.

Table 9 Summary of ConWep [3]

Test	Scaled	Equivalent	ConV	Vep [3]	UF	C [2]
No.	distance(m/kg ^{1/3})	TNT mass	$P_r(MPa)$	$I_r(\text{MPa·ms})$	$P_r(MPa)$	$I_r(MPa\cdot ms)$
		(kg)				
1	0.93	10	6.20	1.33	6.18	1.32
2	0.46	10	35.78	3.49	36.52	3.55

Fig. 24 and Fig. 25 show the probability distributions of P_r and I_r (for 500,000 simulations) under two scaled distances 0.93 m/kg^{1/3} and 0.46 m/kg^{1/3}, respectively. It is observed that the distributions of blast load parameters of P_r and I_r are normally distributed. Under the scaled distance Z=0.93 m/kg^{1/3} and Z=0.46 m/kg^{1/3}, the exceedance probabilities of P_r are 13% and 17%, respectively; the exceedance probabilities of I_r are 32% and 36%, respectively. It is found from the test data and probability analysis that the exceedance probability of peak overpressure and impulse calculated by ConWep under near field blast loads are high, and the values are not conservative, so they cannot meet values of the peak overpressure and impulse in the explosion scene with the higher requirements. Therefore, it may be necessary to propose blast load safety factors of blast loads to satisfy the uncertainty of near-field

651 loading.

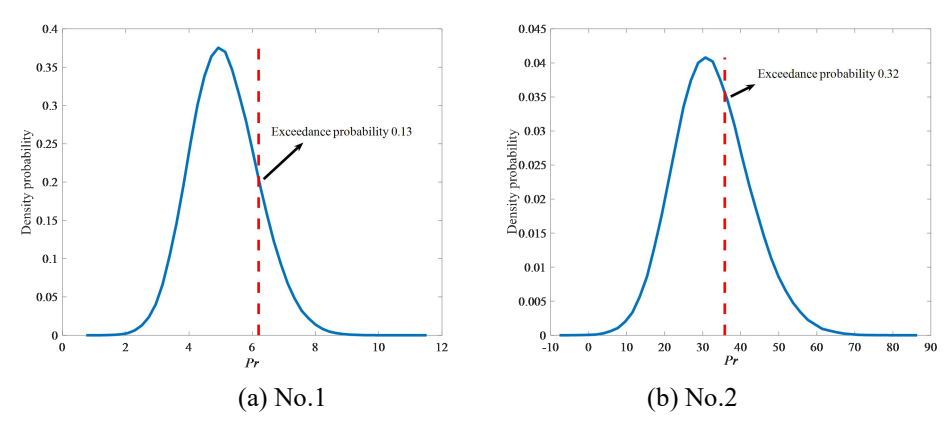
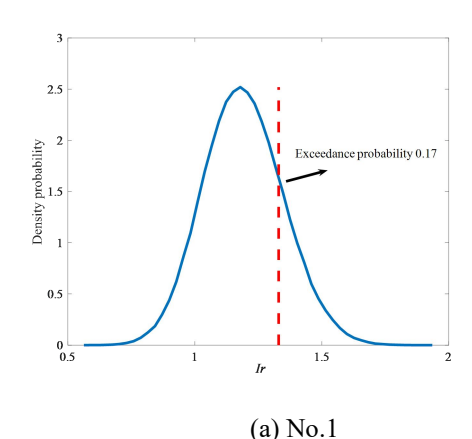


Fig. 24 Probability distribution of peak overpressure Pr for predictive computer code Conwep (n=500000)



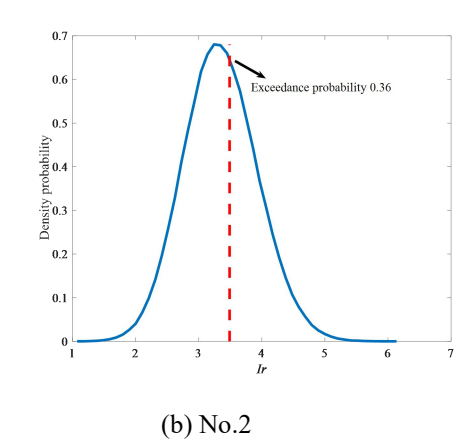
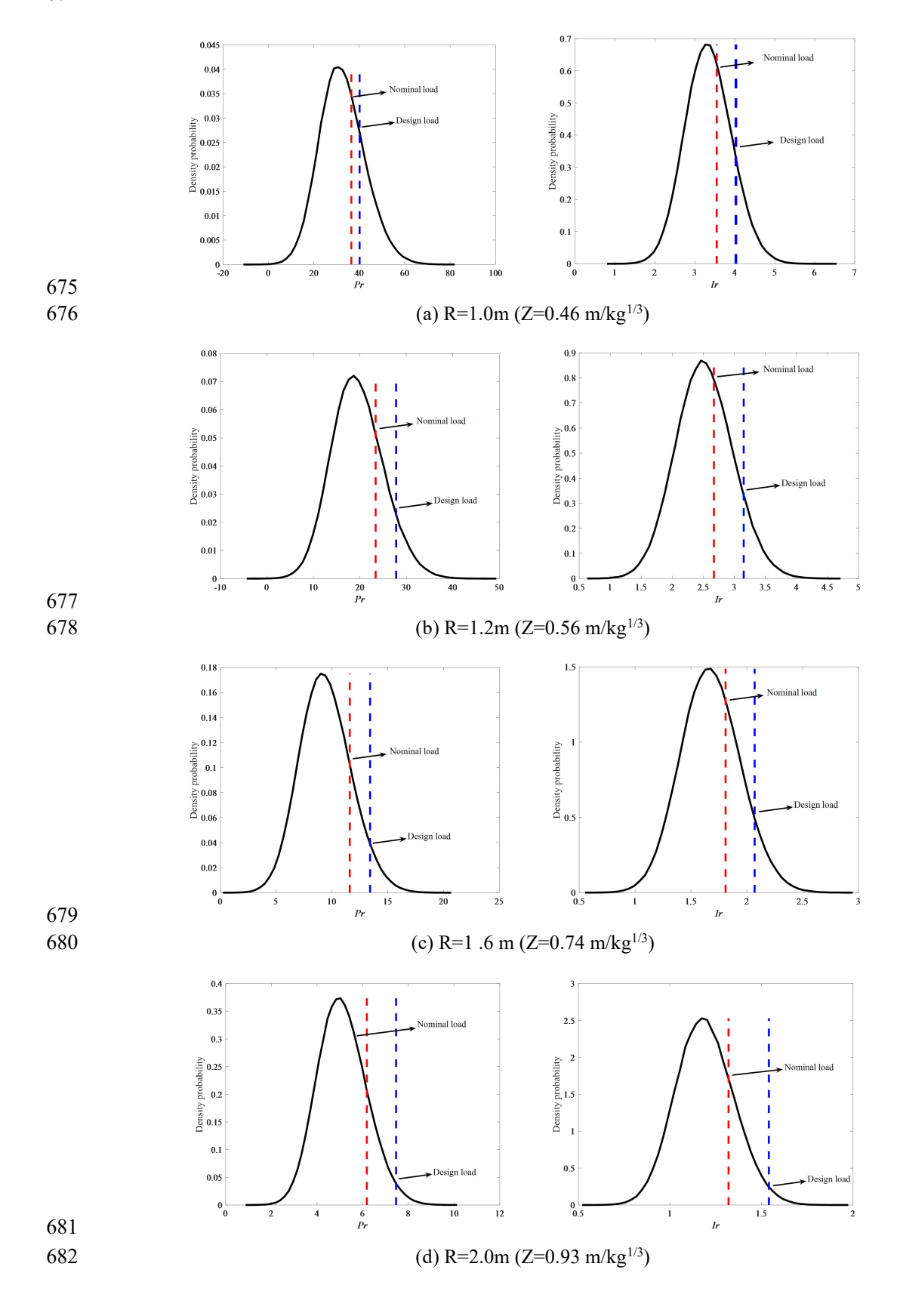


Fig. 25 Probability distribution of impulse *Ir* for predictive computer code Conwep (n=500000)

4.3 Reliability-based safety factor of near-field blast loads

The probability analysis of field blast test in Section 4.2 shows that the near field blast loads are highly uncertain, and the blast loads predicted by ConWep are conservative, which is also suggested in recent experimental work [43]. In order to consider values of blast loads in different blast scenarios, UFC design manual [2] suggests a 20% increase of the charge's TNT equivalent weight in the blast resistance design. However, previous studies [44-45] argue that there seems to be little evidence to support the 20% mass-increase safety factor, this may not be the most appropriate way to deal with uncertainty and blast load variability. Fig. 26 shows the probability distributions of peak overpressure P_r and impulse I_r obtained from PSL-Blast for 10-kg TNT at ranges of 1.0, 1.2, 1.6, 2.0 and 5.0 m. It is observed that reliability level

672



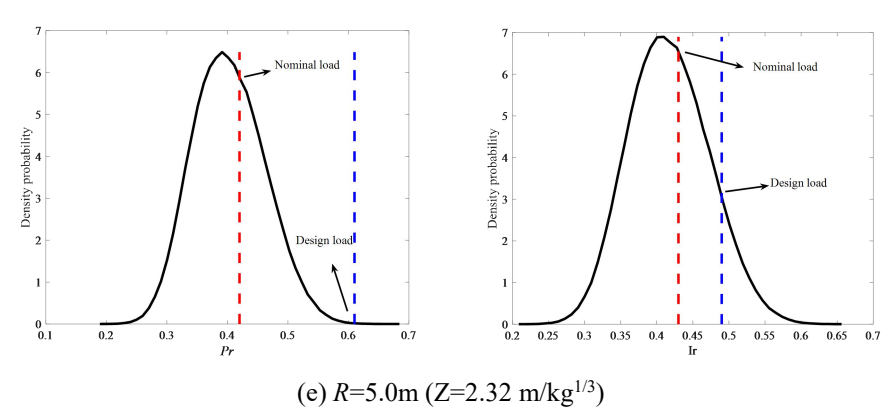


Fig. 26 Exceedance probability of design load considering 20% mass-increase safety factor

686

687

688

689

690

691

692

693

694

695

696

697

698

699

700

701

702

703

704

683

684

685

Tables 10 and Tables 11 lists the reliability levels of design loads calculated in accordance with UFC design manual [2] that includes the 20% mass-increase safety factor for structural design. It is observed that 20% mass-increase safety factor results in reliability levels of 0.81-0.99 and 0.80-0.99 for peak overpressure and impulse, respectively. The reliability level of the design load decreases gradually with decreasing scaled distance. Although the probability that the actual load is greater than the design load is slightly less than the probability that the actual load is greater than the nominal load, the design load considering 20% mass-increase safety factor in the UFC standard does not have a very high level of reliability under near field blast loads as expected. It is noted that this is only the variability of a single blast scenario where W and R are known. If the full spectrum of terrorist threats for a target structure were considered where, for example, W may range from several kilograms to several tonnes, and R from several metres to hundreds of metres, then the variability of blast loading will be significantly greater than the values reported herein. Therefore, before any definitive conclusions can be made about the conservatism (or non-conservatism) of ConWep [3] and other design tools for blast loads, more research is necessary to be conducted to calculate the probability of blast loads in threat scenarios with a larger range of W and R.

705

706

Table 10 Reliability level of peak overpressure considering 20% mass-increase safety factor

Explosive mass of TNT (kg)	Range (m)	Scaled distance (m/kg ^{1/3})	Nominal load (MPa)	Design load including 20% mass-increase safety factor (MPa)	Reliability level
10	1.0	0.46	36.5	40.14	0.81
10	1.2	0.56	23.40	27.81	0.93
10	1.6	0.74	11.6	13.42	0.96
10	2.0	0.93	6.18	7.46	0.98
10	5.0	2.32	0.42	0.61	0.99

Table 11 Reliability level of impulse considering 20% mass-increase safety factor

Explosive mass of TNT (kg)	Range (m)	Scaled distance (m/kg ^{1/3})	Nominal load (Mpa·ms)	Design load including 20% mass-increase safety factor (Mpa·ms)	Reliability level
10	1.0	0.46	3.55	4.03	0.90
10	1.2	0.56	2.67	3.15	0.92
10	1.6	0.74	1.81	2.07	0.94
10	2.0	0.93	1.32	1.54	0.97
10	5.0	2.32	0.43	0.49	0.91

The aforementioned research shows that the reliability level of the design load considering the 20% mass-increase safety factor in the UFC standard is relatively low under the near field blast loads. In order to satisfy the value of blast loads in threat scenes with different reliability levels, the reliability-based safety factor of blast loads is proposed. Some decision makers may be more interested in the 0.50 reliability (mean) blast load given that the threat scenario may already be a conservative (or worst-case) estimate of explosive mass or range. The military may be more interested in ensuring that there is 95% certainty of damaging a military target and so might be interested in a lower reliability level (such as 0.05 or 0.25 of blast load). Table 12 and Table 13 show the reliability-based safety factors of peak overpressure and impulse from *PSL-Blast* under different scaled distances. It is observed that there is a 0.9 reliability level of blast loads with safety factors close to 1.0. To achieve a higher reliability level, a higher safety factor is required. As shown in Table 12 and Table 13, the safety factor of peak overpressure and impulse in the case of 0.05 reliability level

can be as low as 0.44 and 0.65, respectively; the safety factor of peak overpressure and impulse in the case of 0.99 reliability level can be as high as 1.49 and 1.34, respectively. Meanwhile, an increase in scaled distance results in safety factors which are relatively insensitive to reliability level, reflective of the observation that larger scaled distances exhibit smaller variability of blast loads. According to the safety factors of blast loads given in Table 12 and Table 13, designers can select certain peak overpressure and impulse values based on a certain reliability level, which provides an evidenced and risk-based approach to the specification of blast loading.

Table 12 Reliability-based safety factors of peak overpressure

		<u> </u>		1	1	
Reliability	Z=0.5	Z=1.0	Z=1.5	Z=2.0	Z=2.5	Z=3.0
level λ	$(m/kg^{1/3})$	$(m/kg^{1/3})$	$(m/kg^{1/3})$	$(m/kg^{1/3})$	$(m/kg^{1/3})$	$\left(m/kg^{1/3}\right)$
0.05	0.44	0.56	0.66	0.71	0.73	0.74
0.25	0.66	0.70	0.79	0.83	0.85	0.86
0.50	0.82	0.81	0.89	0.93	0.94	0.94
0.90	1.00	0.93	1.00	1.03	1.04	1.04
0.95	1.29	1.11	1.16	1.18	1.19	1.17
0.99	1.49	1.24	1.27	1.29	1.28	1.26

Table 13 Reliability-based safety factors of impulse

Reliability	Z=0.5	Z=1.0	Z=1.5	Z=2.0	Z=2.5	Z=3.0
level λ	$(m/kg^{1/3})$	$(m/kg^{1/3})$	$(m/kg^{1/3})$	$(m/kg^{1/3})$	$(m/kg^{1/3})$	$(m/kg^{1/3})$
0.05	0.65	0.69	0.63	0.73	0.75	0.71
0.25	0.81	0.79	0.73	0.84	0.87	0.81
0.50	0.92	0.87	0.81	0.93	0.95	0.90
0.90	1.04	0.95	0.90	1.02	1.05	0.99
0.95	1.22	1.07	1.02	1.15	1.18	1.12
0.99	1.34	1.15	1.10	1.24	1.27	1.21

5. Summary and conclusions

In this paper, a finite element model of air and TNT is established and validated against existing experimental data, in order to investigate the characteristics of blast waves generated by non-standard charges, namely stochastic shapes and detonator location. The numerical study was designed to emulate hydrodynamic surface instabilities observed in experimental testing of near-field explosions, and the influence rule of stochastic charge shape and detonator location is statistically

- analysed between scaled distances of 0.4 to 3.0 m/kg^{1/3}. Through the established
- 747 computational procedure, probabilistic analysis of blast load parameters from
- experiment tests is carried out. Finally, the reliability level of design load from UFC
- design manual is estimated and the safety factor of blast loads with different reliability
- 750 levels for *PSL-Blast* is suggested.
- 751 The main findings are as follows:
- 752 (1) A stochastic alogrithm of finite element is proposed to provide an innovative
- method for the uncertainty analysis of blast load in the numerical simulation.
- 754 (2) The peak overpressure and impulse of blast loads induced by fireball surface
- 755 instability are normally distributed.
- 756 (3) The peak overpressure and impulse of blast loads induced by stochastic detonator
- 757 location are uniformly distributed.
- 758 (4) The reliability level of the peak overpressure and impulse of blast loads
- considering 20% mass-increase safety factor in the UFC design manual gradually
- decreases with a decrease in scaled distance, and hence reveal a lower reliability
- of near-field blast load parameters.
- 762 (5) The reliability level of peak overpressure and impulse with safety factor of blast
- loads close to 1.0 is approximately 0.90. A decrease in scaled distance intensifies
- the uncertainty of blast, and the interdependency between safety factor and
- reliability level increases.
- 766 Acknowledgements
- 767 The authors gratefully acknowledge the support from the National Natural Science
- 768 Foundation of China under grant numbers 51878445, 51938011, 52178498 and
- 769 52325807.

References:

- 771 [1] Kingery CN, Bulmash G. Air blast parameters from TNT spherical air burst for
- and hemispherical surface burst. BRL Technical Report ARBRL-TR-02555, 1984,
- US Army Armament Research and Development Center, Ballistic Research
- Laboratory, Aberdeen, MD.
- 775 [2] US Army Corps of Engineers. Structures to resist the effects of accidental

- explosions. Air force civil engineer support agency. 2nd ed. UFC 3-340-02, 2014.
- 777 [3] CONWEP. Conventional Weapons Effects Program. US Waterways Experimental
- 778 Station 1991, Vicksburg.
- 779 [4] LSDYNA. LSDYNA Keyword User's Manual: Livermore Software Technology
- 780 Corporation. 2007.
- 781 [5] Brode HL. Numerical Solutions of Spherical Blast Waves. Journal of Applied
- 782 Physics 1955; 26(6): 766-775.
- 783 [6] Yan CS, Wang N, Cui J, Li CH, Zhang XJ. Experimental and numerical
- investigation of charge shape effect on blast load induced by near-field explosions.
- Process Safety and Environmental Protection 2022; 165: 266-277.
- 786 [7] Xiao WF, Andrae M, Gebbeken N. Effect of charge shape and initiation
- configuration of explosive cylinders detonating in free air on blast-resistant
- design. Journal of Structural Engineering, 2020; 146(8): 04020146.
- 789 [8] Rigby SE, Osborne C, Langdon GS, Cooke SB, Pope DJ. Spherical equivalence
- of cylindrical explosives: Effect of charge shape on deflection of blast-loaded
- 791 plates. International Journal of Impact Engineering 2021; 155:103892.
- 792 [9] Tang L, Bird D, Rigby SE, Tyas A. Reflections on variability of blast pressure
- measurement at different scales. The 17th international symposium on the
- interaction of the effects of munitions with structures, 2017, Bad
- 795 Neuenahr-Ahrweiler, Germany.
- 796 [10] Shi Y, Stewart MG. Spatial reliability analysis of explosive blast load damage to
- reinforced concrete columns. Structural Safety 2015; 53: 13-25.
- 798 [11] Stewart MG, Li J. Risk-based assessment of blast-resistant design of ultra-high
- performance concrete columns. Structural Safety 2021; 88: 102030.
- 800 [12] Liu Y, Hao H, Hao YF. Blast fragility analysis of RC columns considering
- chloride-induced corrosion of steel reinforcement. Structural Safety 2022;
- 802 96:102200.
- 803 [13] Stewart MG, Netherton MD. Security Risks And Probabilistic Risk Assessment
- of Glazing Subject to Explosive Blast Loading. Reliability Engineering and
- 805 System Safety 2008; 93(2): 627–638.

- 806 [14] Netherton MD, Stewart MG. The Effects of Explosive Blast Load Variability on
- Safety Hazard and Damage Risks for Monolithic Window Glazing. International
- 308 Journal of Impact Engineering 2009; 36(12): 1346–1354.
- 809 [15] Tyas A. Blast loading from high explosive detonation: what we know and don't
- know. The 13th international conference on shock and impact loads on structures,
- 811 2019, Guangzhou, China.
- 812 [16] Rae PJ, McAfee JM. The blast parameters spanning the fireball from large
- hemispherical detonations of C-4. Propellants Explosives Pyrotechnics 2018;
- 814 43(7): 694–702.
- 815 [17] Twisdale LA, Sues RH, Lavelle FM. Reliability-based design methods for
- protective structures. Structural Safety 1994; 15(1-2): 17–33.
- [18] Low HY, Hao H. Reliability analysis of direct shear and flexural failure modes of
- RC slabs under explosive loading. Engineering Structures 2002; 24(2): 189–198.
- 819 [19] Bogosian D, Ferritto J, Shi Y. Measuring uncertainty and conservatism in
- simplified blast models. The 30th Explosives Safety Seminar, 2002, Atlanta,
- 821 USA.
- 822 [20] Netherton MD, Stewart MG. Blast load variability and accuracy of blast load
- prediction models. International Journal of Protective Structures 2010; 1(4):
- 824 543–570.
- 825 [21] Rigby SE, Sielicki PW. An investigation of TNT equivalence of hemispherical
- PE4 charges. Engineering Transactions 2014; 62(4): 423–435.
- 827 [22] Rigby SE, Tyas A, Fay SD, Clarke SD, Warren JA. Validation of semi-empirical
- blast pressure predictions for far field explosions is there inherent variability in
- blast wave parameters? The 6th international conference on protection of
- structures against hazards, 2014, Tianjin, China.
- 831 [23] Tyas A, Reay JJ, Fay SD, Clarke SD, Rigby SE, Warren JA, Pope DJ.
- Experimental studies of the effect of rapid afterburn on shock development of
- near-field explosions. International Journal of Protective Structures 2016; 7(3):
- 834 452-465.

- 835 [24] Bogosian D, Yu A, Dailey T. Statistical variation in reflected air blast parameters
- from bare charges. The 23rd international symposium on military aspects of blast
- and shock, 2014, Oxford, England.
- 838 [25]Ohrt A, Dailey T, Bogosian D. Statistical variation of air blast parameters from
- bare and cased explosive cylinders. The 22nd international symposium on
- military aspects of blast and shock 2014, Bourges, France.
- [26] Rigby SE, Knighton R, Clarke SD, Tyas A. Reflected near-field blast pressure
- measurements using high speed video. Experimental Mechanics 2020; 60(7):
- 843 875–888.
- 844 [27] Schoutens JE. Review of Large HE Charge Early-Time Detonation Anomalies.
- Technical Report DASIAC SR 182, 1979, Washington, DC.
- 846 [28] Rayleigh. Investigation of the character of the equilibrium of an incompressible
- heavy fluid of variable density. Proceedings of the London Mathematical Society
- 848 1882; 14(1): 170–177.
- [29] Taylor GI. The instability of liquid surfaces when accelerated in a direction
- perpendicular to their planes. II. Proceedings of the Royal Society of London.
- Series A. Mathematical and Physical Sciences 1950; 202(1068): 81–96.
- 852 [30] Meshkov EE. Instability of the interface of two gases accelerated by a shock
- 853 wave. Fluid Dynamics 1969; 4(5): 101–104.
- 854 [31] Richtmyer RD. Taylor instability in shock acceleration of compressible fluids.
- Communications on Pure and Applied Mathematics 1960; 13(2): 297–319.
- 856 [32] Schwer L, Teng H, Souli M. LS-DYNA Air Blast Techniques: Comparisons with
- Experiments for Close-in Charges. The 10th European LS-DYNA Conference
- 858 2015, Würzburg, Germany.
- 859 [33] Huang Y, Willford M, Schwer L. Validation of LS-DYNA MMALE with Blast
- Experiments. The 12th International LS-DYNA Users Conference 2012.
- 861 [34] Antoci C, Gallati M, Sibilla S. Numerical simulation of fluid–structure interaction
- by SPH. Computers & Structures 2007; 85(11–14): 879-890.
- [35] Børvik T, Olovsson L, Hanssen AG, Dharmasena KP, Hansson H, Wadley HNG.
- A discrete particle approach to simulate the combined effect of blast and sand

- impact loading of steel plates. Journal of the Mechanics and Physics of Solids
- 866 2011, 59(5): 940-958.
- 867 [36] Rigby S, Fuller B, Tyas A. Validation of near-field blast loading in LS-DYNA.
- The 5th International Conference on Protective Structures 2018, Poznan, Poland.
- [37] Aquelet N, Souli M. 2D to 3D ALE Mapping. 10th International LS-DYNA Users
- 870 Conference 2008.
- [38] Lapoujade V, Dorsselaer NV, Kevorkian S, Cheval K. A Study of Mapping
- Technique for Air Blast Modeling. The 11th International LS-DYNA Users
- 873 Conference 2010.
- [39] Kalra A, Feng Z, Yang KH, King AI. Key Parameters in Blast Modeling Using
- 2D to 3D ALE Mapping Technique. The 13th International LS-DYNA Users
- 876 Conference 2012.
- [40] Hu Y, Chen L, Fang Q, Xiang HB. Blast Loading Model of the RC Column under
- 878 Close-in Explosion induced by the Double-end-initiation Explosive Cylinder.
- 879 Engineering structures 2018; 175: 304-321.
- 880 [41] Wu C, Fattori G, Whittaker A. Investigation of air-blast effects from
- spherical-and cylindrical-shaped charges. International Journal of Protective
- 882 Structures 2010; 1: 345–62.
- 883 [42] Rigby SE, Tyas A, Bennett T, Clarke SD, Fay SD. The negative phase of the blast
- load. International Journal of Protective Structures 2014; 5(1): 1–20.
- 885 [43] Barr AD, Rigby SE, Clarke SC, Farrimond D, Tyas A. Temporally and spatially
- resolved reflected overpressure measurements in the extreme near field. Sensors
- 887 2023; 23(2): 964.
- 888 [44] Stewart MG, Netherton MD. Reliability-based design load factors for explosive
- blast loading. Journal of Performance of Construct Facilities 2015; 29(5):
- 890 B4014010.
- 891 [45] Stewart MG. Reliability-based load factor design model for explosive blast
- loading. Structural Safety 2018; 71:13-23.